Transparent Image Layer Diffusion using Latent Transparency

Lvmin Zhang and Maneesh Agrawala Stanford University

We present LayerDiffusion, an approach enabling large-scale pretrained latent diffusion models to generate transparent images. The method allows generation of single transparent images or of multiple transparent layers. The method learns a "latent transparency" that encodes alpha channel transparency into the latent manifold of a pretrained latent diffusion model. It preserves the production-ready quality of the large diffusion model by regulating the added transparency as a latent offset with minimal changes to the original latent distribution of the pretrained model. In this way, any latent diffusion model can be converted into a transparent image generator by finetuning it with the adjusted latent space. We train the model with 1M transparent image layer pairs collected using a human-in-the-loop collection scheme. We show that latent transparency can be applied to different open source image generators, or be adapted to various conditional control systems to achieve applications like foreground/background-conditioned layer generation, joint layer generation, structural control of layer contents, etc. A user study finds that in most cases (97%) users prefer our natively generated transparent content over previous ad-hoc solutions such as generating and then matting. Users also report the quality of our generated transparent images is comparable to real commercial transparent assets like Adobe Stock.

1 Introduction

While large-scale models for generating images have become foundational in computer vision and graphics, surprisingly little research attention has been given to layered content generation or transparent image generation. This situation is in stark contrast to substantial market demand. The vast majority of visual content editing software and workflows are layer-based, relying heavily on transparent or layered elements to compose and create content.

The primary factors contributing to this research gap are the lack of training data and the difficulty in manipulating the data representation of existing large-scale image generators. High-quality transparent image elements on the Internet are typically hosted by commercial image stocks with limited (and costly) access, in contrast to text-image datasets that already include billions of images (e.g., LAION [38]). The largest open-source transparent image datasets are often less than 50K in size (e.g., DIM [53] includes 45,500 transparent images). Meanwhile, most open-source image generation models, e.g., Stable Diffusion, are latent diffusion models that are sensitive to their latent space data representations. Even minor changes to the latent distribution could severely degrade inference or finetuning. For instance, Stable Diffusion 1.5 and XL use different latent spaces, and finetuning with mismatched latents can cause significant degradation in output image quality [44]. This adds to the challenge of manipulating the data representation of existing models to support additional formats like transparent images.

We present a "latent transparency" approach that enables large-scale pretrained latent diffusion models to generate transparent images as well as multiple transparent layers. This method encodes image transparency into a latent offset that is explicitly regulated to avoid disrupting the latent distribution. The latent transparency is encoded and decoded by external independent models, ensuring that the original pretrained latent encoder/decoder is perfectly preserved, so as to maintain high-quality results

"Woman with messy hair, in the bedroom"



"Burning firewood, on a table, in the countryside"

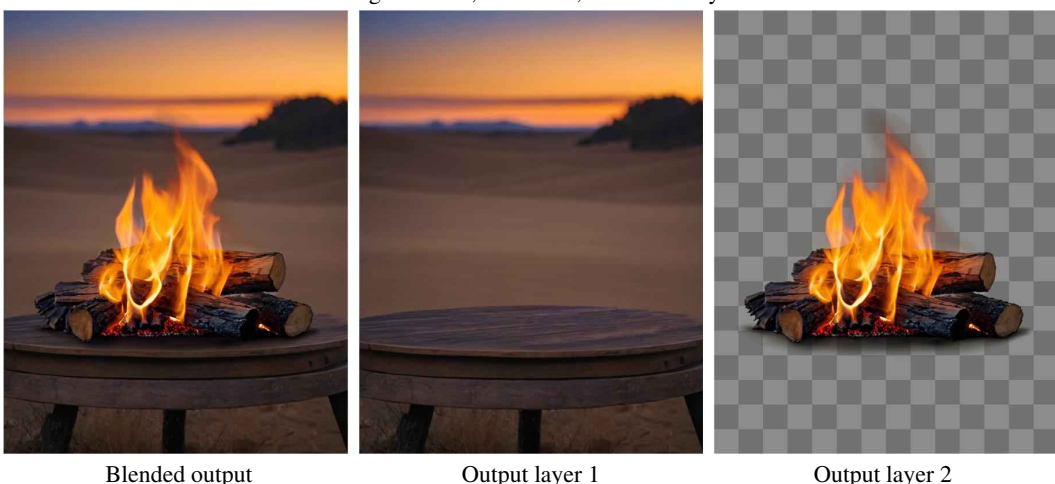


Figure 1: Generating transparent images and layers. For the given text prompts (top), our framework is capable of generating multiple layers with transparency. These layers can be blended to produce images corresponding to the prompts. Zoom in to see details including messy hair and semi-transparent fire.

of state-of-the-art diffusion models. To generate multiple layers together, we use a shared attention mechanism to ensure consistency and harmonious blending between image layers, and train LoRAs to adapt the models to different layer conditions.

We employ a human-in-the-loop scheme to train our framework and collect data simultaneously. We finalize the scale of our dataset at 1M transparent images, covering a diversity of content topics and styles. We then use state-of-the-art methods to extend the dataset to multi-layer samples. This dataset not only enables the training of transparent image generators but can also be used in different applications like background/foreground-conditioned generation, structure-guided generation, style transfer, *etc*.

Experiments show that in a dominant majority of cases (97%), users prefer the transparent content generated natively by our method over previous ad-hoc solutions like generating-then-matting. When we compare the quality of our generated results with the search results from commercial transparent assets sites like Adobe Stock, user preference rates suggest that quality is comparable.

In summary, we (1) propose "latent transparency", an approach to enable large-scale pretrained latent diffusion models to generate single transparent images or multiple transparent layers, (2) present a shared attention mechanism to generate layers with consistent and harmonious blending, (3) present a dataset containing transparent images and layers collected using a human-in-the-loop scheme, (4)

present a pretrained model for transparent image generation and two pretrained LoRAs for multiple layer generation.

2 Related Work

2.1 Hiding Images inside Perturbations

Research in multiple fields point out a phenomenon: neural networks have the ability to "hide" features in perturbations inside existing features without changing the overall feature distributions, e.g., hiding an image inside another image through small, invisible pixel perturbations. A typical CycleGAN [60] experiment showcases face-to-ramen, where the human face identity could be hidden in a ramen picture. Similarly, invertible downscaling [52] and invertible grayscale [51] indicate that neural networks can hide a large image inside a smaller one, or hide a colorful image inside a grayscale one, and then reconstruct the original image. In another widely verified experiment Goodfellow et al. [14] show that adversarial example signals can be hidden inside feature perturbations to influence the behaviors of other neural networks. In this paper, our proposed "latent transparency" utilizes similar principles: hiding image transparency features inside a small perturbation added to the latent space of Stable Diffusion [43], while at the same time avoiding changes to the overall distribution of the latent space. This enables a seamless transition from existing non-transparent image diffusion models to transparent diffusion models, and eases further fine-tuning.

2.2 Diffusion Probabilistic Models and Latent Diffusion

Diffusion Probabilistic Model [40] and related training and sampling methods like Denoising Diffusion Probabilistic Model (DDPM) [16], Denoising Diffusion Implicit Model (DDIM) [41], and score-based diffusion [42] contribute to the foundations of recent large-scale image generators. Early image diffusion methods usually directly use pixel colors as training data [41, 36, 24]. Recently Latent Diffusion Model (LDM) [34] has been proposed for easier training and lowering the computation requirements. This method has been further extended to create Stable Diffusion [43]. Even more recently, eDiff-I [6] uses an ensemble of multiple conditions including a T5 text encoder [32], a CLIP text and image embedding encoder [19]. Versatile Diffusion [54] adopts a multi-purpose diffusion framework to process text, an image, and variations within a single model. To achieve richer functionality, Composer [18] uses a joint training method with various control signals over the pretrained image diffusion model conditioned on image embedding. Mixture-of-Experts (MoEs) methods [39, 12] also contribute to the models of text-to-image generation.

2.3 Customized Diffusion Models and Image Editing

Early methods to customize diffusion models have focused on text-guidance [30, 21, 5, 7, 20, 33, 15]. Image diffusion algorithms also naturally support inpainting [33, 5]. Textual Inversion [13] and DreamBooth [35] can personalize the contents of generated results based on a small set of examplar images of the same topic or object. Recently, control models have also been used to add additional conditions for the generation of text-to-image models, *e.g.*, ControlNet [58], lightweight T2I-adapter [29], etc. Uni-ControlNet [59] proposes a multi-scale condition injection strategy to learn an adapter for various local controls to reduce the training computation costs. SeeCoder [55] presents a semantic context encoder to replace the original text encoder to generate image variants. IP-Adapter [57] uses a cross-attention mechanism to separate text and image features, allowing for the control signals of the reference image as a visual prompt. More recently researchers [50, 27] have proposed portrait personalization methods using one or more face images. Experiments show that our approach can be combined with various control models or customization methods to generate transparent layers for different applications.

2.4 Transparent Image Processing

Transparent image processing is closely related to image decomposition, layer extraction, color palette processing, as well as image matting [49, 2, 1]. Typical color-based decomposition can be viewed as a RGB color space geometry problem [45, 46, 47, 48, 11]. These ideas have also been extended to more advanced blending of image layers [25]. Unmixing-based color separation also

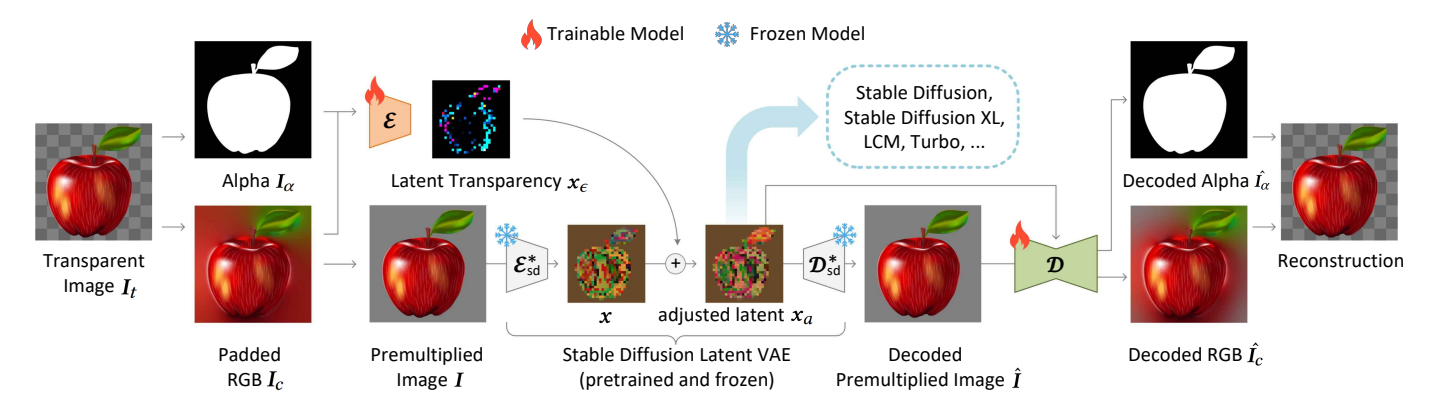


Figure 2: Latent Transparency. Given an input transparent image, our framework encode a "latent transparency" to adjust the latent space of Stable Diffusion. The adjusted latent images can be decoded to reconstruct the color and alpha. This latent space with transparency can be further used in training or fine-tuning pretrained image diffusion models.

contributes to image decomposition [3], and semantic features can be used in image soft segmentation [4]. We compare our approach to several state-of-the-art deep-learning based matting methods in our experiments and discussion. *PPMatting* [9] is a neural network image matting model trained from scratch using standard matting datasets. *Matting Anything* [26] is a image matting model using the Segment Anything Model (SAM) [22] as a backbone. *VitMatte* [56] is a trim-map-based matting method using Vision Transformer (ViT).

3 Method

Our approach enables a Latent Diffusion Model (LDM), like Stable Diffusion, to generate transparent images, and then further extend the model to jointly generate multiple transparent layers together. In section 3.1, we introduce the method to adjust the LDM latent space to support transparent image encoding/decoding. In section 3.2, we adapt pretrained latent diffusion models with the adjusted latent space to generate transparent images. In section 3.3, we describe the method for joint or conditional layer generating. Finally, we detail the dataset preparation and implementation details of neural network training in section 3.4.

Definitions To clarify the presentation we first define some terms. For any transparent image $I_t \in \mathbb{R}^{h \times w \times 4}$ with RGBA channels, we denote the first 3 RGB color channels as $I_c \in \mathbb{R}^{h \times w \times 3}$ and the alpha channel as $I_\alpha \in \mathbb{R}^{h \times w \times 1}$. Since the colors are physically undefined at pixels where the alpha value is strictly zero, in this paper, all undefined areas in I_c are always padded by an iterative Gaussian filter (Appendix A) to avoid aliasing and unnecessary edge patterns. We call I_c the "padded RGB image" (Fig. 2). The I_t can be converted to a "premultiplied image" as $I = I_c * I_a$ where * denotes pixelwise multiplication. In this paper, all RGB values are in range [-1,1] (consistent with Stable Diffusion) while all alpha values are in range [0,1]. The premultiplied image I can be seen as a common non-transparent RGB image that can be processed by any RGB-formatted neural networks. Visualizations of these images are shown in Fig. 2.

3.1 Latent Transparency

Our goal is to add transparency support to large-scale latent diffusion models, like Stable Diffusion (SD), that typically uses a latent encoder (VAE) to convert RGB images to latent images before feeding it to a diffusion model. Herein, the VAE and the diffusion model should share the same latent distribution, as any major mismatch can significantly degrade the inference/training/fine-tuning of the latent diffusion framework. When we adjust the latent space to support transparency, the original latent distribution must be preserved as much as possible. This seemingly ill-defined objective can be determined by a straight-forward measurement: we can check how well the modified latent distribution can be decoded by the original pretrained frozen latent decoder — if decoding a modified latent image creates severe artifacts, the latent distribution is misaligned or broken.

We can write this "harmfulness" measurement mathematically as follows. Given an RGB image I, the pretrained and frozen Stable Diffusion latent encoder $\mathcal{E}^*_{sd}(\cdot)$ and decoder $\mathcal{D}^*_{sd}(\cdot)$, where the * indicates frozen models, we denote the latent image as $x = \mathcal{E}^*_{sd}(I)$. Assuming this latent image x is modified by any offset x_ϵ , produces an adjusted latent $x_a = x + x_\epsilon$. The decoded RGB reconstruction can then be written as $\hat{I} = \mathcal{D}^*_{sd}(x_a)$ and we can evaluate how "harmful" the offset x_ϵ is as

$$\mathcal{L}_{\text{identity}} = ||\boldsymbol{I} - \hat{\boldsymbol{I}}||_2 = ||\boldsymbol{I} - \mathcal{D}_{sd}^*(\mathcal{E}_{sd}^*(\boldsymbol{I}) + \boldsymbol{x}_{\epsilon})||_2,$$
(1)

where $||\cdot||_2$ is the L2 norm distance (mean squared error). Intuitively, if $\mathcal{L}_{identity}$ is relatively high, the $\boldsymbol{x}_{\epsilon}$ could be harmful and may have destroyed the reconstruction functionality of SD encoder-decoder, otherwise if $\mathcal{L}_{identity}$ is relatively low, the offset $\boldsymbol{x}_{\epsilon}$ does not break the latent reconstruction and the modified latent can still be handled by the pretrained Stable Diffusion.

We make use of the latent offset x_{ϵ} to establish "latent transparency" for encoding/decoding transparent images. More specifically, we train from scratch a latent transparency encoder $\mathcal{E}(\cdot,\cdot)$ that takes the RGB channels I_c and alpha channel I_{α} as input to convert pixel-space transparency into a latent offset

$$\boldsymbol{x}_{\epsilon} = \mathcal{E}(\boldsymbol{I}_{c}, \boldsymbol{I}_{\alpha}). \tag{2}$$

We then train from scratch another latent transparency decoder $\mathcal{D}(\cdot,\cdot)$ that takes the adjusted latent $x_a = x + x_\epsilon$ and the aforementioned RGB reconstruction $\hat{I} = \mathcal{D}_{sd}^*(x_a)$ to extract the transparent image from the adjusted latent space

$$[\hat{I}_c \ \hat{I}_\alpha] = \mathcal{D}(\hat{I}, x_a), \tag{3}$$

where \hat{I}_c , \hat{I}_α are the reconstructed color and alpha channels. The neural network layer architecture of $\mathcal{E}(\cdot,\cdot)$ and $\mathcal{D}(\cdot,\cdot)$ is in Appendix B. We evaluate the reconstruction with

$$\mathcal{L}_{\text{recon}} = ||\boldsymbol{I_c} - \hat{\boldsymbol{I}_c}||_2 + ||\boldsymbol{I_a} - \hat{\boldsymbol{I}_a}||_2, \tag{4}$$

and we experimentally find that the result quality can be further improved by introducing a PatchGAN discriminator loss

$$\mathcal{L}_{\text{disc}} = \mathbb{L}_{\text{disc}}([\hat{I}_c, \hat{I}_a]), \tag{5}$$

where $\mathbb{L}_{disc}(\cdot,\cdot)$ is a GAN objective from a 5-layer patch discriminator (Appendix C). The final objective can be jointly written as

$$\mathcal{L}_{\text{vae}} = \lambda_{\text{recon}} \mathcal{L}_{\text{recon}} + \lambda_{\text{identity}} \mathcal{L}_{\text{identity}} + \lambda_{\text{disc}} \mathcal{L}_{\text{disc}},$$
 (6)

where $\lambda_{...}$ are weighting parameters: by default we use $\lambda_{\text{recon}} = 1$, $\lambda_{\text{identity}} = 1$, $\lambda_{\text{disc}} = 0.01$. By training this framework with \mathcal{L}_{vae} , the adjusted latent x_a can be encoded from transparent images or vise versa, and those latent images can be used in fine-tuning Stable Diffusion. We visualize the pipeline in Fig. 2.

3.2 Diffusion Model with Latent Transparency

Since the altered latent space with latent transparency is explicitly regulated to align with the original pretrained latent distribution (Eq. 1), Stable Diffusion can be directly fine-tuned on the altered latent space. Given the adjusted latent x_a , diffusion algorithms progressively add noise to the image and produces a noisy image x_t , with t denoting how many times noise is added. When t is large enough, the latent image approximates pure noise. Given a set of conditions including the time step t and text prompts c_t , image diffusion algorithms learn a network ϵ_θ that predicts the noise added to the noisy latent image x_t with

$$\mathcal{L} = \mathbb{E}_{\boldsymbol{x}_t, t, \boldsymbol{c}_t, \epsilon \sim \mathcal{N}(0, 1)} \left[\| \epsilon - \epsilon_{\theta}(\boldsymbol{x}_t, t, \boldsymbol{c}_t)) \|_2^2 \right]$$
 (7)

where \mathcal{L} is the overall learning objective of the entire diffusion model. This training is visualized in Fig. 3-(a).

3.3 Generating Multiple Layers

We further extend the base model to a multi-layer model using attention sharing and LoRAs [17], as shown in Fig. 3-(b). We denote the foreground noisy latent as x_f and background as x_b , and train two LoRAs, a foreground LoRA parameterized by θ_f and a background LoRA by θ_b , to denoise the

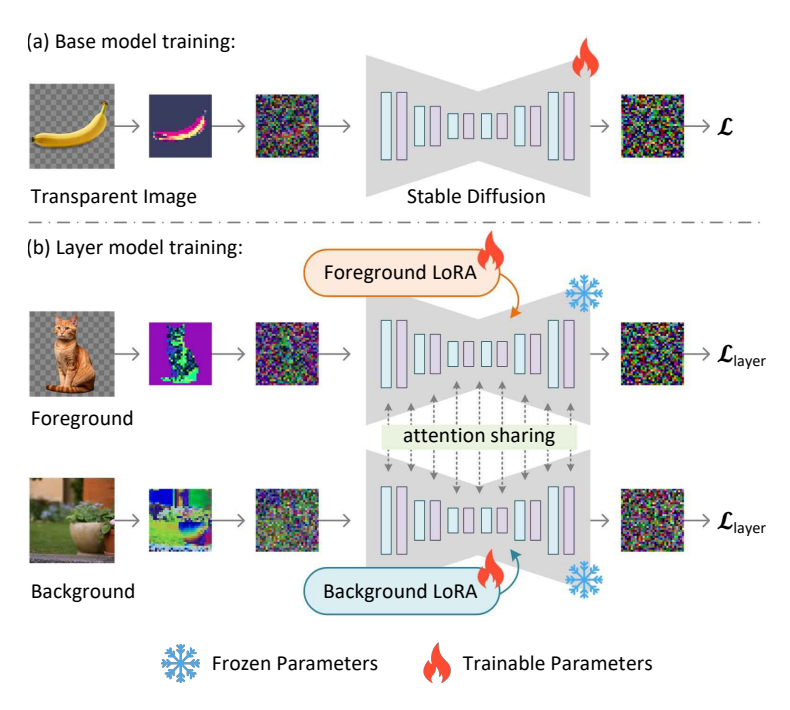


Figure 3: **Model Training.** We visualize the training of the base model to generate transparent images, and the training of the multi-layer model to generate multiple layers together. When training the base diffusion model (a), all model weights are trainable, whereas for training the multi-layer model (b), only two LoRAs are trainable (the foreground LoRA and background LoRA).

latent images. If the two models independently denoise the two images, we have the two objectives with

$$\begin{cases}
\mathbb{E}_{\boldsymbol{x}_{f},t,\boldsymbol{c}_{t},\epsilon_{f} \sim \mathcal{N}(0,1)} \left[\|\epsilon_{f} - \epsilon_{\theta,\theta_{f}}(\boldsymbol{x}_{f},t,\boldsymbol{c}_{t}))\|_{2}^{2} \right] \\
\mathbb{E}_{\boldsymbol{x}_{b},t,\boldsymbol{c}_{t},\epsilon_{b} \sim \mathcal{N}(0,1)} \left[\|\epsilon_{b} - \epsilon_{\theta,\theta_{b}}(\boldsymbol{x}_{b},t,\boldsymbol{c}_{t}))\|_{2}^{2} \right]
\end{cases}$$
(8)

where ϵ_f , ϵ_b are latent noise for the foreground and background. We then merge the two independent diffusion process to achieve coherent generation. For each attention layer in the diffusion model, we concatenate all {key, query, value} vectors activated by the two images, so that the two passes can be merged into a jointly optimized big model $\epsilon_{\theta,\theta_f,\theta_g}(\cdot)$. We denote the merged noise as concatenated $\epsilon_m = [\epsilon_f, \epsilon_b]$, and we have the final objective

$$\mathcal{L}_{\text{layer}} = \mathbb{E}_{\boldsymbol{x}_f, \boldsymbol{x}_b, t, \boldsymbol{c}_t, \epsilon_m \sim \mathcal{N}(0, 1)} \left[\| \epsilon_m - \epsilon_{\theta, \theta_f, \theta_g}(\boldsymbol{x}_f, \boldsymbol{x}_b, t, \boldsymbol{c}_t)) \|_2^2 \right]$$
(9)

to coherently generate multiple layers together. We can also make simple modifications to this objective to support conditional layer generation (e.g., foreground-conditioned background generation or background-conditioned foreground generation). More specifically, by using a clean latent for the foreground instead of noisy latent (i.e., by always setting $\epsilon_f = 0$), the model will not denoise foreground, and the framework becomes a foreground-conditioned generator. Similarly, by setting $\epsilon_b = 0$, the framework becomes a background-conditioned generator. We implement all these conditional variations in experiments.

We also introduce several alternative architectures in Fig. 4 for more complicated workflows. We can add zero-initialized channels to the UNet and use VAE (with or without latent transparency) to encode foreground, or background, or layer combinations into conditions, and train the model to generate foreground or background (*e.g.*, Fig. 4-(b, d)), or directly generate blended images (*e.g.*, Fig. 4-(a, c)).

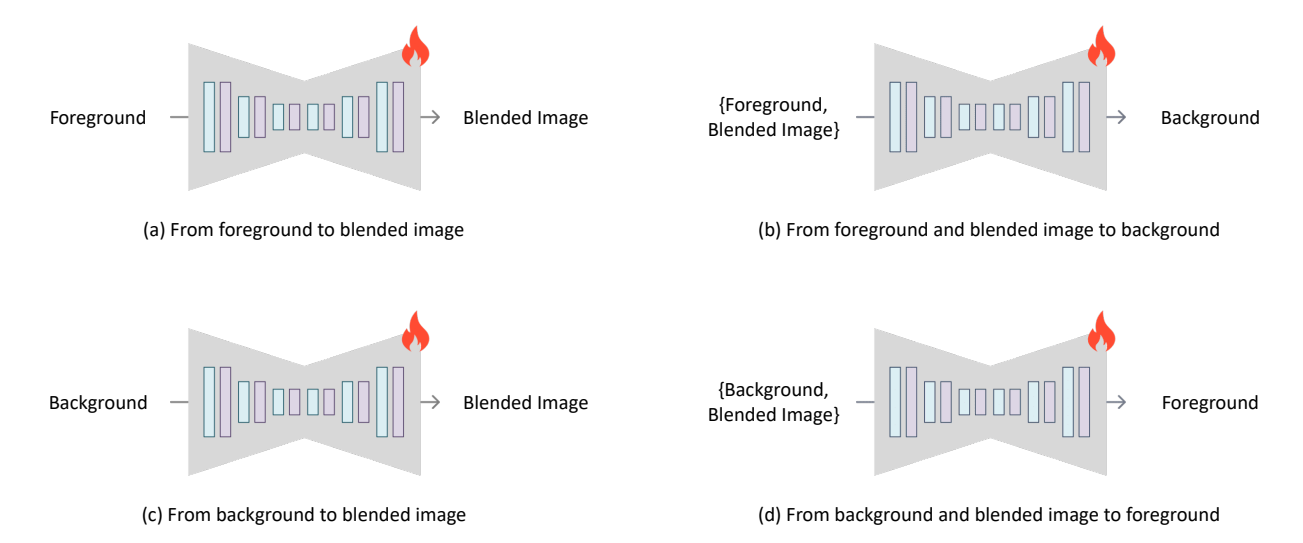


Figure 4: **Alternative Architectures for More Complicated Workflows.** We also include several alternative models for more complicated workflows. These include generating a blended image from background or foreground, as well as generating background/foreground from other combined layers.

3.4 Dataset Preparation and Training Details

Base Dataset We use a human-in-the-loop method to collect a dataset of transparent images and train our models. The dataset initially contains 20k high-quality transparent PNG images purchased or downloaded free from 5 online image stocks (all images include commercial use permission (examples in Fig. 5-(a)). We then train the SDXL VAE with latent transparency using randomly sampled images with equal probability (at batch size 8), and then train the SDXL diffusion model using the same data with adjusted latents. Next we repeat the following steps for a total of 25 rounds. At the beginning of each round, we generate 10k random samples using the last model in the previous round. and the random prompts from LAIONPOP [37]. We then manually pick 1000 samples to add back to the training dataset. The newly added samples are given a 2x higher probability of appearing in training batches in the next round. We then train the latent transparency encoder-decoder and diffusion models again. After 25 rounds, the size of the dataset increases to 45K. Afterwards, we generate 5M sample pairs without human interaction and use the LAION Aesthetic threshold [38] setting of 5.5 and clip score sorting to obtain 1M sample pairs. We automatically remove samples that do not contain any transparent pixels as well as those that do not contain any visible pixels. Finally, all images are captioned with LLaVA [28] (an open-source multi-modal GPT similar to GPT4v) to get detailed text prompts. The training of both the VAE and the diffusion model is finalized with another 15k iterations using the final 1M dataset.

Multi-layer Dataset We further extend our $\{text, transparent image\}$ dataset into a $\{text, foreground layer, background layer\}$ dataset, so as to train the multi-layer models. As shown in Fig. 5-(b), we ask GPTs (we used ChatGPT for 100k requests and then moved to LLAMA2 for 900k requests) to generate structured prompts pairs for foreground like "a cute cat", entire image like "cat in garden", and background like "nothing in garden" (we ask GPT to add the word "nothing" to the background prompt). The foreground prompt is processed by our trained transparent image generator (Section 3.2) to obtain the transparent images. Then, we use Diffusers Stable Diffusion XL Inpaint model [10] to inpaint all pixels with alpha less than one to obtain intermediate images using the prompt for the entire images. Finally, we invert the alpha mask, erode k=8 pixels and inpaint again with the background prompt to get the background layer. We repeat this process 1M times to generate 1M layer pairs.

Training Details We use the AdamW optimizer at learning rate 1e-5 for both VAE and diffusion model. The pretrained Stable Diffusion model is SDXL [31]. For the the LoRA [17] training, we always use rank 256 for all layers. We use the Diffusers' standard for naming and extracting LoRA keys. In the human-in-the-loop data collection, each round contains 10k iterations at batch size 16.

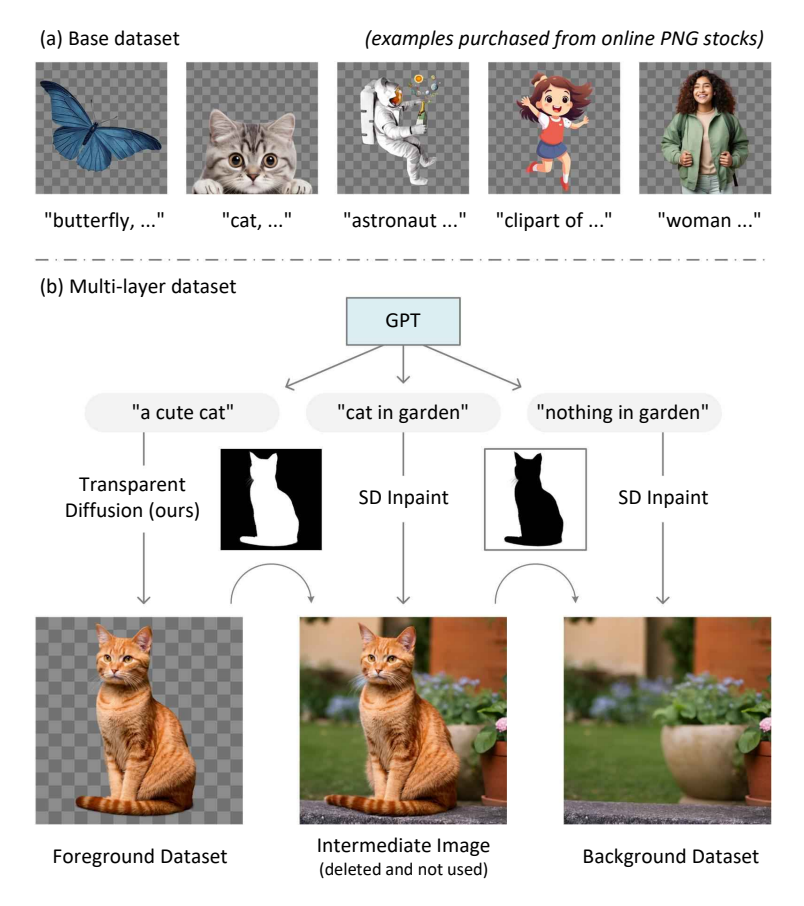


Figure 5: **Dataset Preparation.** We demonstrate the preparation of the two dataset: the transparent image dataset (base dataset) and multi-layer dataset. The base dataset is collected by downloading online transparent images with the help of a human-in-the-loop training method. The multi-layer dataset is synthesized with our transparent diffusion model and several state-of-the-art models including ChatGPT, SDXL inpaint model, *etc.* The final scale of each dataset is around 1M.

The training devices are 4x A100 80G NV-link, and the entire training takes one week (to reduce budget, the training is paused when human are collection data for the next round of optimization) and the real GPU time is about 350 A100 hours. Our approach is training friendly for personal-scale or lab-scale research as the 350 GPU hours can often be processed within 1K USD.

4 Experiments

We detail qualitative and quantitative experiments with our system. We first present qualitative results with single images (Section 4.1), multiple layers (Section 4.2), as well as iterative generation (Section 4.3), and then show that our framework can also be combined with control modules for wider applications (Section 4.4). We then analysis the importance of each component with ablative study (Section 4.5), and then discuss the difference and connection between our approach and image matting (Section 4.6). Finally, we conduct perceptual user study (Section 4.7) and present a range of discussions to further study the behaviors of our framework (Section 4.8,4.9,4.10).

4.1 Qualitative Results

We present qualitative results in Fig. 6 with a diverse set of transparent images generated using our single-image base model. These results showcase the model's capability to generate *natively* transparent images that yield high-quality glass transparency, hair, fur, and semi-transparent effects



Figure 6: **Qualitative Results.** We showcase various examples of transparent images generated by our model. The prompts for each group is given at the top of the examples. These examples only use our base single-layer model.

like glowing light, fire, magic effect, *etc*. These results also demonstrate the model's capability to generalize to diverse content topics.

We further present multi-layer results in Fig. 7 with transparent layers generated by our multi-layer model and the blended images. These results showcase the model's capability to generate harmonious compositions of objects that can be blended together seamlessly. The layers are not only consistent with respect to illumination and geometric relationships, but also demonstrate the aesthetic quality of Stable Diffusion (*e.g.*, the color choice of the background and foreground follows a learned distribution that looks harmonious and aesthetic).

4.2 Conditional Layer Generation

We present conditional layer generation results (*i.e.*, foreground-conditioned background and background-conditioned foreground generation) in Fig. 8, We can see that the model is able to generate consistent composition with coherent geometry and illumination. In the "bulb in the church" example, the model tries to generate a aesthetic symmetric design to match the foreground. The "sitting on bench"/"sitting on sofa" examples demonstrate that the model is able to infer the interaction between foreground and background and generate corresponding geometry.

4.3 Iterative Generation

Fig. 9 shows that we can iteratively use the background-conditioned foreground generation model to achieve composition or arbitrary number of layers. For each new layer, we blend all previously generated layers into one RGB image and feed it to the background-conditioned foreground model. We also observe that the model is able to interpret natural language in the context of the background image, *e.g.*, generating a book in front of the cat. The model displays strong geometric composition capabilitites, *e.g.*, composing a human sitting on a box.

4.4 Controllable Generation

As shown in Fig. 10, we demonstrate that existing control models like ControlNet [58] can be applied to our model for enriched functionality. We can see that the model is able to preserve the global

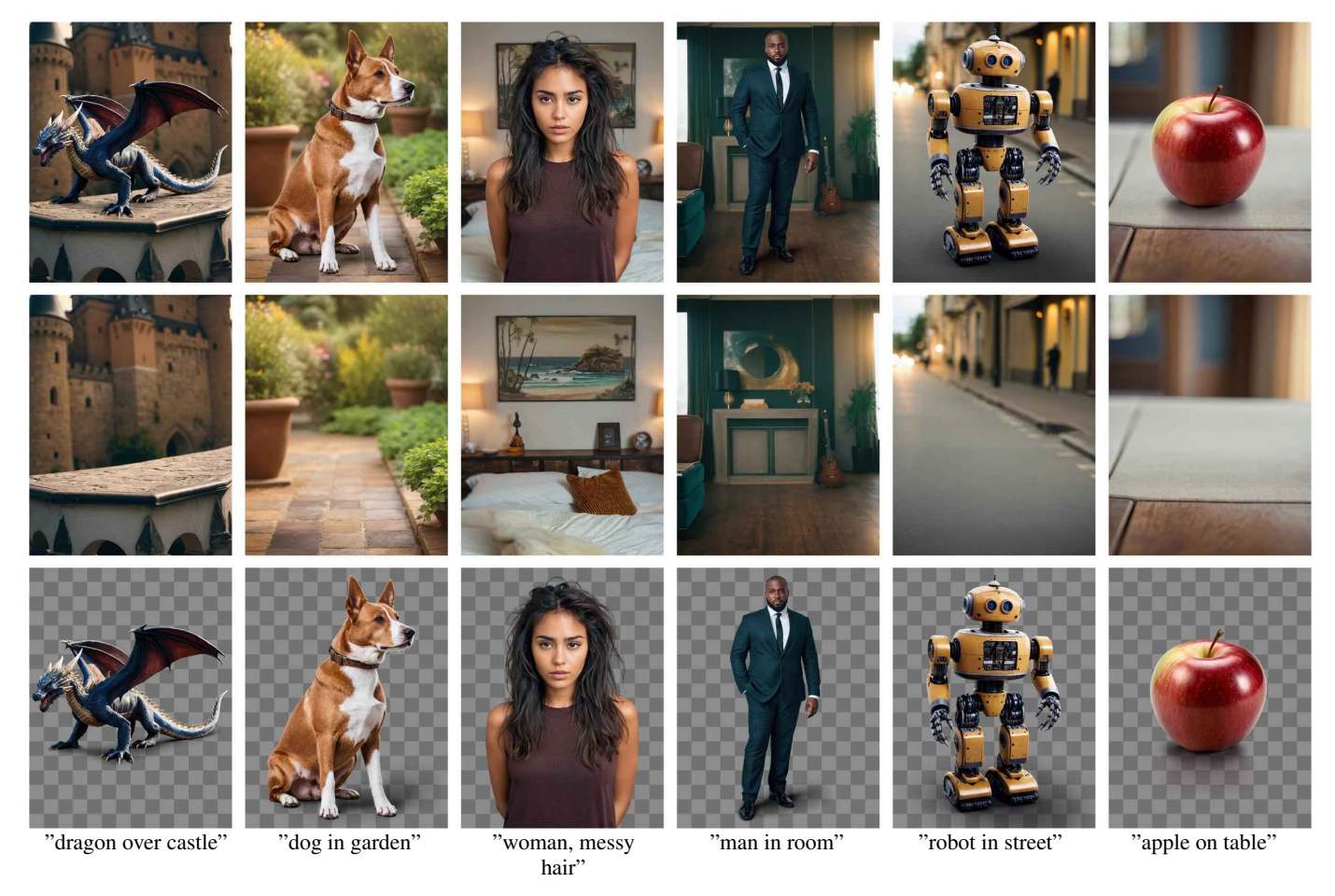


Figure 7: **Multi-Layer Qualitative Results.** We presents qualitative results generated by our model using prompts with diverse topics. For each example, we show the blended image, and two output layers. More results are available in supplementary materials.

structure according to the ControlNet signal to generate harmonious compositions with consistent illumination effects. We also use a "reflective ball" example to show that the model is able to interact with the content of the foreground and background to generate consistent illumination like the reflections.

4.5 Ablative Study

We conduct an ablative study to evaluate the contribution of each component in our framework. We are interested in a possible architecture that does not modify Stable Diffusion's latent VAE encoder/decoder, but only add channels to the UNet. In the original Stable Diffusion, a $512 \times 512 \times 3$ image is encoded to a latent image of size $64 \times 64 \times 4$. This indicates that if we duplicate the $512 \times 512 \times 1$ alpha channel 3 times into a $512 \times 512 \times 3$ matrix, the alpha could be directly encoded into a $64 \times 64 \times 4$ latent image. By concatenating this with the original latent image, the final latent image would form a a $64 \times 64 \times 8$ matrix. This means we could add 4 channels to Stable Diffusion UNet to force it support an alpha channel. We present the results of this approach in Fig. 11-(a). We can see that this method severely degrades the generation quality of the pretrained large model, because its latent distribution is changed; although the VAE is unchanged (it is frozen), the additional 4 channels significantly change the feature distribution after the first convolution layer in the VAE UNet. Note that this is different from adding a control signal to the UNet — the UNet must generate and recognize the added channels all at the same time because diffusion is a iterative process, and the outputs of any diffusion step become the input of the next diffusion step.

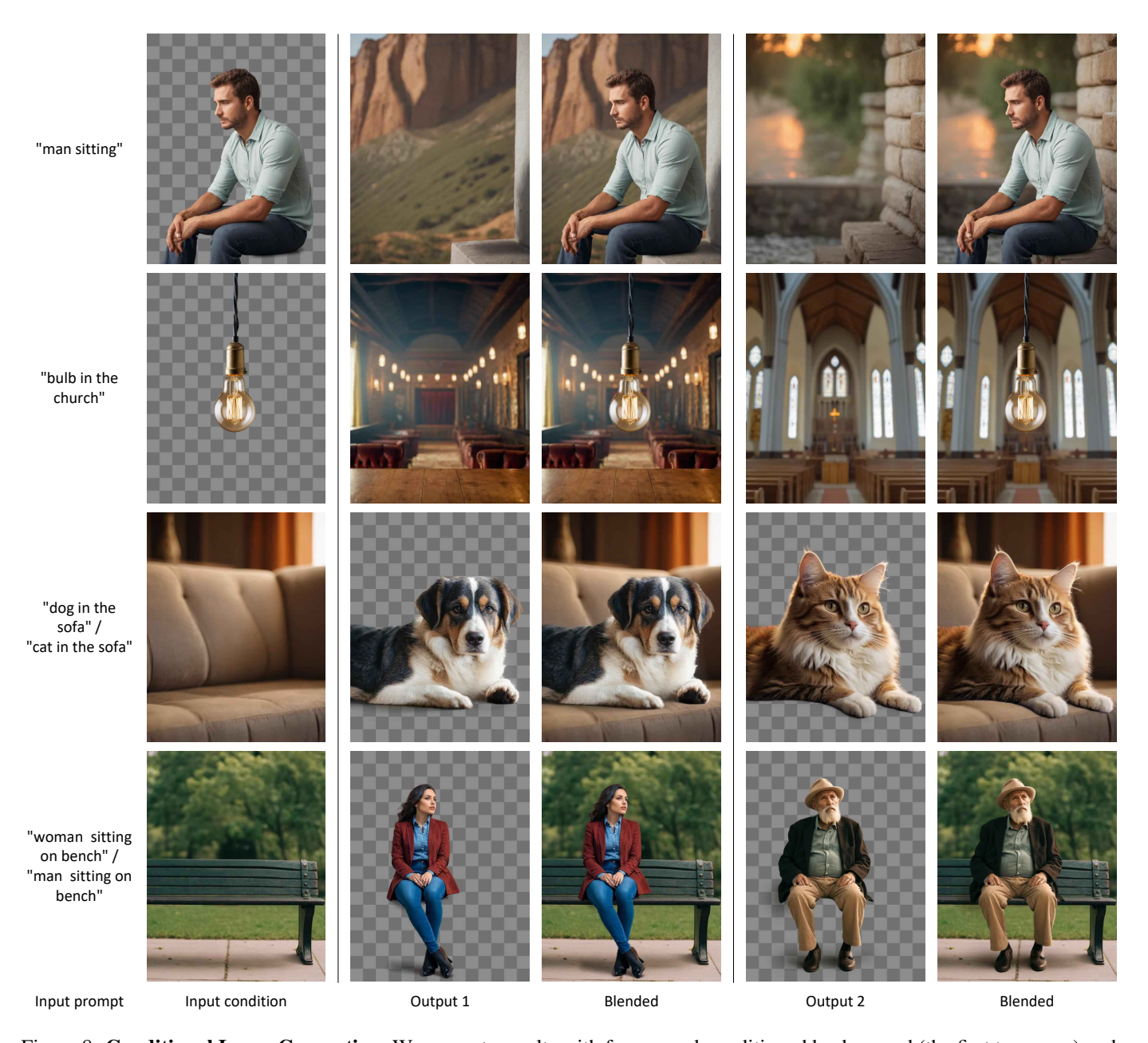


Figure 8: **Conditional Layer Generating.** We presents results with foreground-conditioned background (the first two rows) and background-conditioned foreground (the last two rows). For each example, we generate two foregrounds/backgrounds.

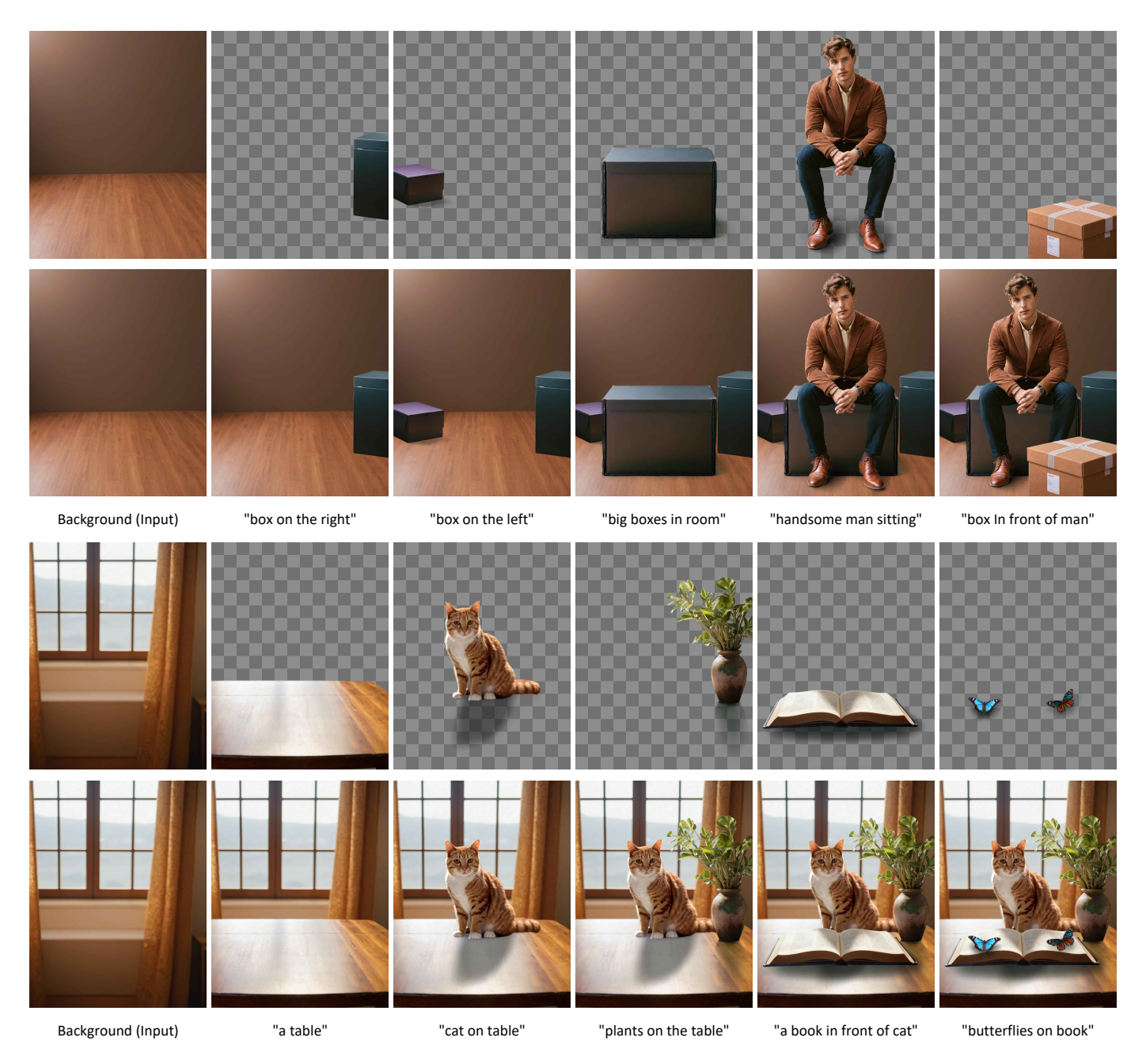


Figure 9: **Generating Multiple Layers.** We show that our framework can compose multiple layers iteratively, by repeating the background-conditioned foreground model. At each step, we blend all existing layers and feed the blended result to the background-conditioned generator. The prompts at each step is at the bottom of outputs.



Figure 10: **Combining with Control Models.** We show that our approach can directly be combined with control models like ControlNet [58] to enhance the functionality. The prompts are "human in street", "human in forest", "big reflective ball in street", and "big reflective ball in forest".

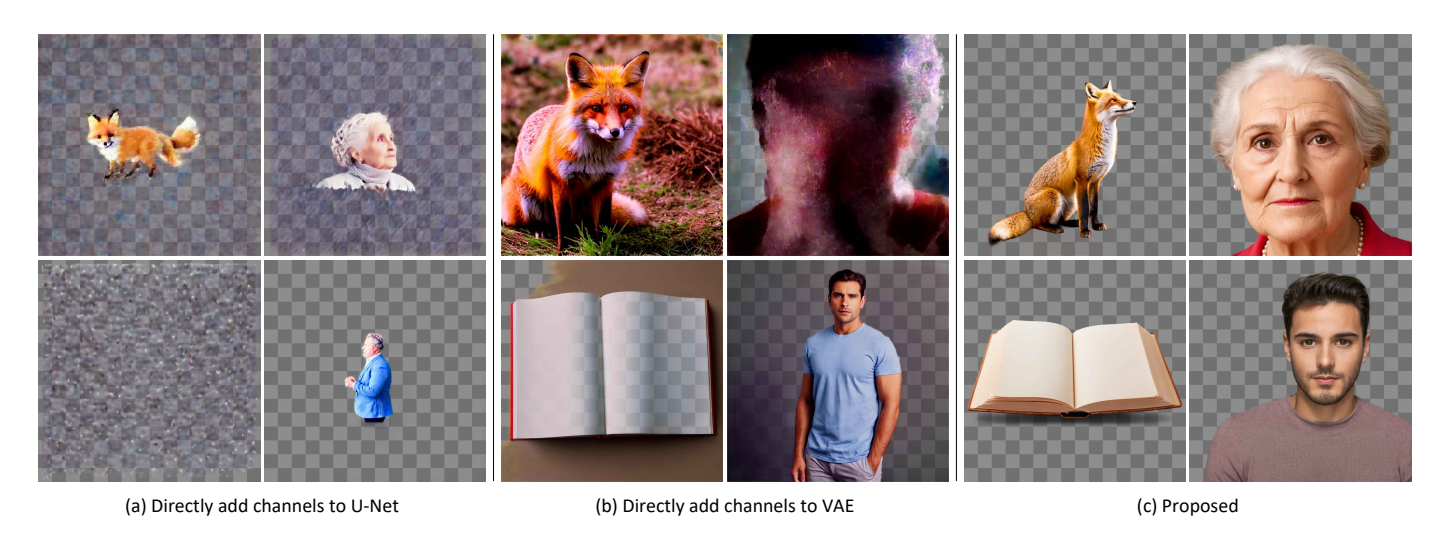


Figure 11: **Ablative Study.** We compare our approach to two alternative architecture: directly adding channels to UNet and directly adding channels to VAE. When adding channel to UNet, we directly encode alpha channel as an external image and add 4 channels to UNet. When adding channels to VAE, the UNet is finetuned on the latent images encoded by the newer VAE. The test prompts are "fox", "elder woman", "a book", "man".

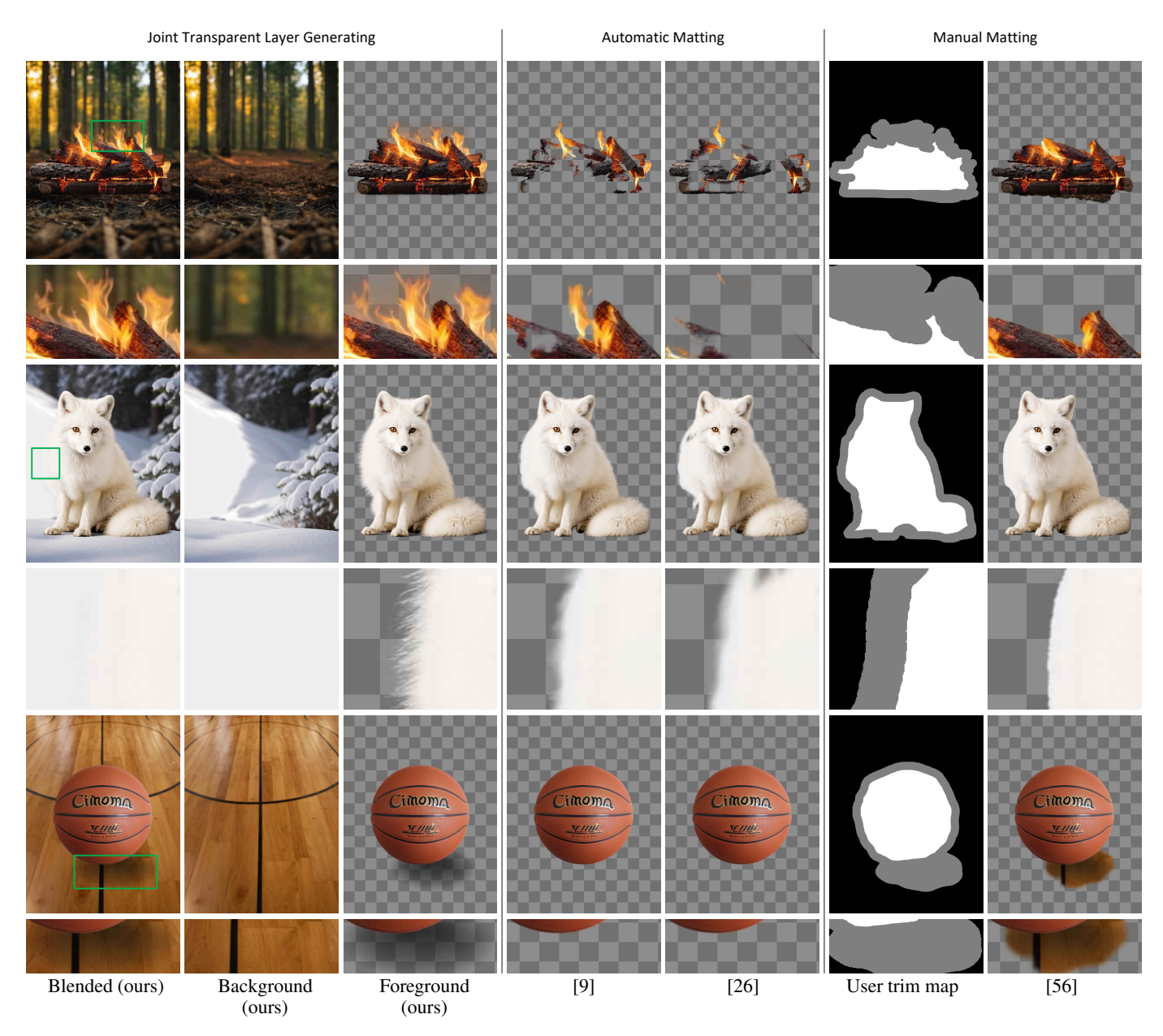


Figure 12: **Difference between Joint Layer Generating and Generating-then-matting.** This is *not* a result comparison since the left-most images are outputs, and our method does not decompose images. We presents our jointly generated layers on the left and try to reproduce similar results using matting approaches. The prompts are "fire on burning wood in forest", "white fox in white snow ground, all white, very white", and "basketball".

Table 1: **User Study.** We present the results from user study. We conduct user study in two groups: the first group compares outputs between different methods, while the second group directly compare our generated results to the search result of a commercial transparent image assets (Adobe Stock). Higher is better and best in bold.

Candidate	Group 1	Group 2
SD + PPMatting [9]	$2.1{\pm}1.2\%$	/
SD + Matting Anything [26]	$0.8 {\pm} 0.5\%$	/
Ours (base model)	$97.1 \pm 1.9\%$	$45.3 \pm 9.1\%$
Commercial Transparent Asset Stock	/	54.7±8.3%

In Fig. 11-(b), we test another architecture that directly adds a channel to the VAE encoder and decoder. We train the VAE to include an alpha channel, and then further train the UNet. We observe that such training is very unstable, and the results suffer from different types of collapse from time to time. The essential reason leading to this phenomenon is that the latent distribution is changed too much during in the VAE fine-tuning.

4.6 Relationship to Image Matting

We discuss the difference and connection between native transparent image generation and image matting. To be specific, we test the following matting methods: (1) *PPMatting* [9] is a state-of-the-art neural network image matting model. This model reports to achieve the highest precision among all "classic" neural network based matting methods, *i.e.*, neural models trained from scratch on a collected dataset of transparent images. This model is fully automatic and does not need a user-specified tri-map. (2) *Matting Anything* [26] is a new type of image matting model based on the recently released Segment Anything Model (SAM) [22]. This model uses pretrained SAM as a base and finetunes it to perform matting. This model also does not need a user-specified tri-map. We also include a tri-map-based method to study the potential for user-guided matte extraction. (3) *VitMatte* [56] is a state-of-the-art matting model that uses trim maps. The architecture is a Vision Transformer (ViT) and represents the highest quality of current user-guided matting models.

As shown in Fig. 12, we can see that several types of patterns are difficult for matting approaches, *e.g.*, semi-transparent effects like fire, pure white fur against a pure white background, shadow separation, *etc*. For semi-transparent contents like fire and shadows, once these patterns are blended with complicated background, separating them becomes a nearly impossible task. To obtain perfectly clean elements, probably the only method is to synthesize elements from scratch, using a native transparent layer generator. We further notice the potential to use outputs of our framework to train matting models.

4.7 Perceptual User Study

In order to perceptually evaluate and compare our approach with existing methods, we perform a perceptual user study focusing on human aspects of our native transparent results and ad-hoc method like Stable Diffusion + generation-and-matting. In particular, the user study involves 14 individuals, where 11 individuals are online crowd-source workers, 1 is a computer science student, and the other 2 are professional content creators. We sample 100 results using 3 methods (prompts are randomly sampled from PickaPic [23]), and this leads to 100 result groups, with each group containing 3 results from 3 methods. The participants are invited to rank the results in each group. When ranking the results in each group, we ask users the question – "Which of the following results do you prefer most? Please rank the following transparent elements according to your preference". We use the preference rate as the testing metric. This process is repeated 4 times to compute the standard deviation. Afterwards, we calculate the average preference rate of each method. We call this user study "group 1".

We compare our approach with SD+[9], SD+[26]. Here in, the "SD+" means first using Stable Diffusion XL to generate a RGB image, and then performing matting. Results are shown in Table. 1, group 1. We find that users prefer our approach over all other approaches (in more than 97% cases). This demonstrates the advantage of native transparent image generation over ad-hoc solution like generation-then-matting.



Figure 13: **Raw outputs of the RGB channels and alpha channel.** We present the raw RGB and alpha channel for evaluation. The prompts are "woman with messy hair", "boy with messy hair", and "glass cup".

We also perform another simple user preference experiment, "group 2", to compare our results against the searching for commercial transparent assets from Adobe Stock, using the same aforementioned user preference metric. In Table. 1, group 2, we report that the preference rate of our method is very close to commercial stock (45.3% v.s. 54.7%). Though the high-quality paid content from commercial stock is still preferred marginally. This result indicates that our generated transparent content is competitive to commercial sources that require users to pay for each image.

4.8 Raw RGBA Channels

Fig. 13 shows the raw outputs with each channel in our generated transparent images. We can see that the model avoids aliasing by padding the RGB channel with smooth "bleeding" colors. This approach ensure high-quality foreground color in areas of alpha blending.

4.9 Community Models

As shown in Fig. 14, our method can be applied to various community models, LoRAs, and prompt styles, without additional training. More specifically, we try a Minecraft LoRA, a pixel art LoRA, an anime model [8], and several community prompt styles. We can see that applying to different models neither degrades the quality of target model/LoRAs nor degrades the quality of image

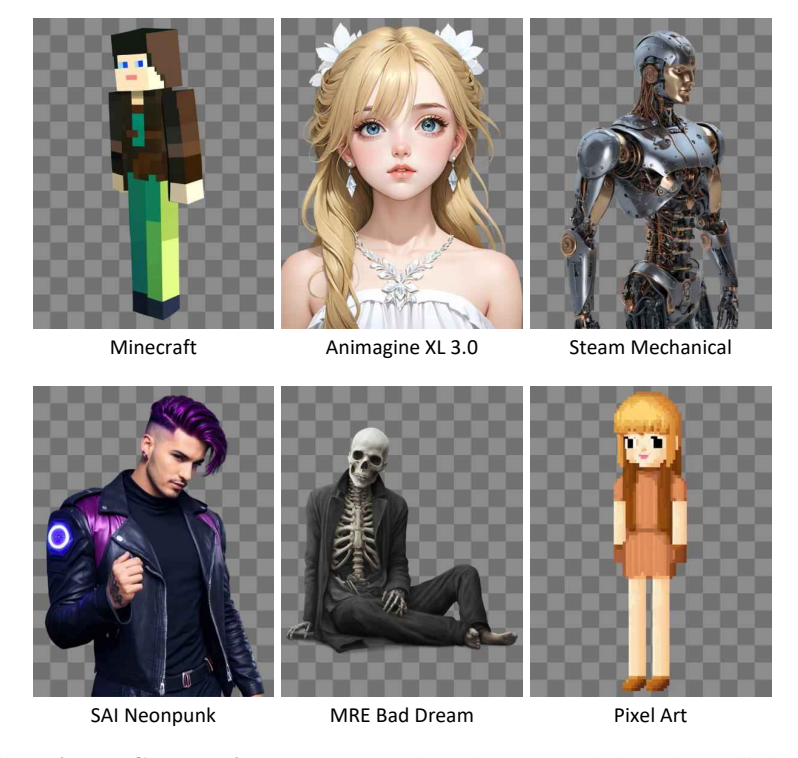


Figure 14: **Applying to Community Models.** We show that our model can be applied to community LoRAs/Models/PromptStyles to achieve diverse results. All images are achieved using prompt "person", excepting Animagine using "1girl, masterpiece, fantastic art".

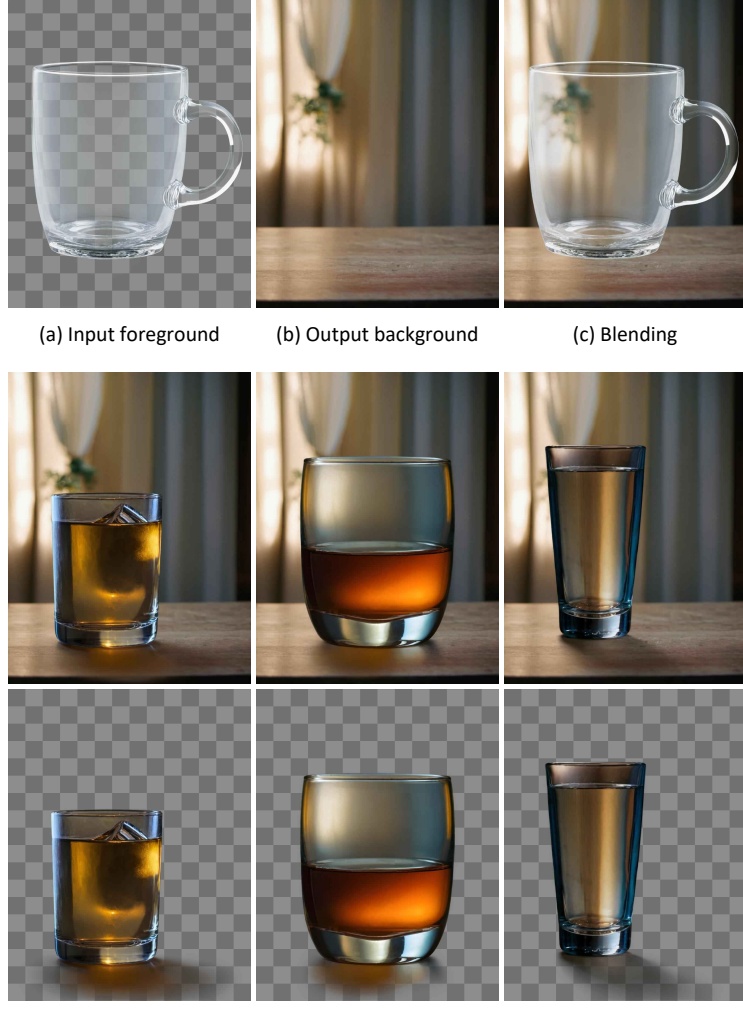
transparency. This integration capability suggests the model potential for wider use in diverse creative and professional domains.

4.10 Limitations

As shown in Fig. 15, one trade-off with our framework is between generating "clean transparent elements" and "harmonious blending". For instance, if the transparent image is a clean and resuable element without any special illumination or shadow effects, generating a background that can be harmoniously blended with the foreground can be very challenging and the model may not succeed in every cases (Fig. 15-(c) is a failure case). This phenomenon can be cured to some extent if we only use backgrounds as conditions to generate foregrounds to force a harmonious blending (Fig. 15-(d)). Nevertheless, this will also lead to illumination influencing the transparent object, making the transparent objects less reusable. One may argue that the image in Fig. 15-(a) is much more reuseable for designers and in-the-wild applications than the transparent images in Fig. 15-(d) which contain many specific patterns bound to the background.

5 Conclusion

In summary, this paper introduces "latent transparency", an approach to create either individual transparent images or a series of coherent transparent layers. The method encodes the transparent alpha channel into the latent distribution of Stable Diffusion. This process ensures that the high-quality output of large-scale image diffusion models, by regulating an offset added to the latent space. The training of the models involved 1M pairs of transparent image layers, gathered using a human-in-the-loop collection scheme. We present a range of applications, such as generating layers conditioned on foreground/background, combining layers, structure-controlled layer generating, etc. User study results indicate that in a vast majority of cases, users favor the transparent content produced natively by our method over traditional methods like generation-then-matting. The quality of the transparent images generated was found to be comparable to the assets in commercial stocks.



(d) Background-conditioned foreground

Figure 15: **Limitation.** The prompt in this example is "glass cup on table in a warm room". If the input foreground is a clean transparent object without any illumination or shadow effects, harmonious blending is very difficult since the alpha blending does not create deformation of light or casting of shadow. This can be resolved to some extent when using the background as a condition to generate the foreground. But in this case, getting a clean and reusable transparent object without the influence of illumination is difficult.

References

- [1] Y. Aksoy, T. O. Aydın, M. Pollefeys, and A. Smolić. Interactive high-quality green-screen keying via color unmixing. *ACM Trans. Graph.*, 35(5):152:1–152:12, 2016.
- [2] Y. Aksoy, T. O. Aydın, and M. Pollefeys. Designing effective inter-pixel information flow for natural image matting. In *Proc. CVPR*, 2017.
- [3] Y. Aksoy, T. O. Aydın, A. Smolić, and M. Pollefeys. Unmixing-based soft color segmentation for image manipulation. *ACM Trans. Graph.*, 36(2):19:1–19:19, 2017.
- [4] Y. Aksoy, T.-H. Oh, S. Paris, M. Pollefeys, and W. Matusik. Semantic soft segmentation. *ACM Trans. Graph. (Proc. SIGGRAPH)*, 37(4):72:1–72:13, 2018.
- [5] O. Avrahami, D. Lischinski, and O. Fried. Blended diffusion for text-driven editing of natural images. In *Proceedings of the IEEE/CVF Conference on Computer Vision and Pattern Recognition*, pages 18208–18218, 2022.
- [6] Y. Balaji, S. Nah, X. Huang, A. Vahdat, J. Song, K. Kreis, M. Aittala, T. Aila, S. Laine, B. Catanzaro, et al. ediffi: Text-to-image diffusion models with an ensemble of expert denoisers. *arXiv preprint arXiv:2211.01324*, 2022.
- [7] T. Brooks, A. Holynski, and A. A. Efros. Instructpix2pix: Learning to follow image editing instructions, 2022.
- [8] cagliostrolab. animagine-xl-3.0. huggingface, 2024.
- [9] G. Chen, Y. Liu, J. Wang, J. Peng, Y. Hao, L. Chu, S. Tang, Z. Wu, Z. Chen, Z. Yu, Y. Du, Q. Dang, X. Hu, and D. Yu. Pp-matting: High-accuracy natural image matting, 04 2022.
- [10] diffusers. stable-diffusion-xl-1.0-inpainting-0.1. diffusers, 2024.
- [11] Z.-J. Du, L.-F. Kang, J. Tan, Y. Gingold, and K. Xu. Image vectorization and editing via linear gradient layer decomposition. *ACM Transactions on Graphics (TOG)*, 42(4), Aug. 2023.
- [12] W. Fedus, B. Zoph, and N. Shazeer. Switch transformers: Scaling to trillion parameter models with simple and efficient sparsity. *The Journal of Machine Learning Research*, 23(1):5232–5270, 2022.
- [13] R. Gal, Y. Alaluf, Y. Atzmon, O. Patashnik, A. H. Bermano, G. Chechik, and D. Cohen-Or. An image is worth one word: Personalizing text-to-image generation using textual inversion. *arXiv* preprint arXiv:2208.01618, 2022.
- [14] I. J. Goodfellow, J. Shlens, and C. Szegedy. Explaining and harnessing adversarial examples. In Y. Bengio and Y. LeCun, editors, 3rd International Conference on Learning Representations, ICLR 2015, San Diego, CA, USA, May 7-9, 2015, Conference Track Proceedings, 2015.
- [15] A. Hertz, R. Mokady, J. Tenenbaum, K. Aberman, Y. Pritch, and D. Cohen-Or. Prompt-to-prompt image editing with cross attention control. *arXiv* preprint arXiv:2208.01626, 2022.
- [16] J. Ho, A. Jain, and P. Abbeel. Denoising diffusion probabilistic models. NeurIPS, 2020.
- [17] E. J. Hu, Y. Shen, P. Wallis, Z. Allen-Zhu, Y. Li, S. Wang, L. Wang, and W. Chen. Lora: Low-rank adaptation of large language models. *arXiv preprint arXiv:2106.09685*, 2021.
- [18] L. Huang, D. Chen, Y. Liu, Y. Shen, D. Zhao, and J. Zhou. Composer: Creative and controllable image synthesis with composable conditions. *arXiv preprint arXiv:2302.09778*, 2023.
- [19] G. Ilharco, M. Wortsman, R. Wightman, C. Gordon, N. Carlini, R. Taori, A. Dave, V. Shankar, H. Namkoong, J. Miller, H. Hajishirzi, A. Farhadi, and L. Schmidt. Openclip, 2021.
- [20] B. Kawar, S. Zada, O. Lang, O. Tov, H. Chang, T. Dekel, I. Mosseri, and M. Irani. Imagic: Text-based real image editing with diffusion models. *arXiv preprint arXiv:2210.09276*, 2022.

- [21] G. Kim, T. Kwon, and J. C. Ye. Diffusionclip: Text-guided diffusion models for robust image manipulation. In *Proceedings of the IEEE/CVF Conference on Computer Vision and Pattern Recognition*, pages 2426–2435, 2022.
- [22] A. Kirillov, E. Mintun, N. Ravi, H. Mao, C. Rolland, L. Gustafson, T. Xiao, S. Whitehead, A. C. Berg, W.-Y. Lo, P. Dollár, and R. Girshick. Segment anything. arXiv:2304.02643, 2023.
- [23] Y. Kirstain, A. Polyak, U. Singer, S. Matiana, J. Penna, and O. Levy. Pick-a-pic: An open dataset of user preferences for text-to-image generation. 2023.
- [24] Z. Kong and W. Ping. On fast sampling of diffusion probabilistic models. CoRR, 2106, 2021.
- [25] Y. Koyama and M. Goto. Decomposing images into layers with advanced color blending. Computer Graphics Forum, 37(7):397–407, Oct. 2018. ISSN 1467-8659. doi: 10.1111/cgf. 13577.
- [26] J. Li, J. Jain, and H. Shi. Matting anything. arXiv: 2306.05399, 2023.
- [27] Z. Li, M. Cao, X. Wang, Z. Qi, M.-M. Cheng, and Y. Shan. Photomaker: Customizing realistic human photos via stacked id embedding. 2023.
- [28] H. Liu, C. Li, Q. Wu, and Y. J. Lee. Visual instruction tuning. In NeurIPS, 2023.
- [29] C. Mou, X. Wang, L. Xie, J. Zhang, Z. Qi, Y. Shan, and X. Qie. T2i-adapter: Learning adapters to dig out more controllable ability for text-to-image diffusion models. arXiv preprint arXiv:2302.08453, 2023.
- [30] A. Nichol, P. Dhariwal, A. Ramesh, P. Shyam, P. Mishkin, B. McGrew, I. Sutskever, and M. Chen. Glide: Towards photorealistic image generation and editing with text-guided diffusion models. arXiv preprint arXiv:2112.10741, 2021.
- [31] D. Podell, Z. English, K. Lacey, A. Blattmann, T. Dockhorn, J. Müller, J. Penna, and R. Rombach. Sdxl: Improving latent diffusion models for high-resolution image synthesis. July 2023.
- [32] C. Raffel, N. Shazeer, A. Roberts, K. Lee, S. Narang, M. Matena, Y. Zhou, W. Li, and P. J. Liu. Exploring the limits of transfer learning with a unified text-to-text transformer. Oct. 2019. doi: 10.48550/ARXIV.1910.10683.
- [33] A. Ramesh, P. Dhariwal, A. Nichol, C. Chu, and M. Chen. Hierarchical text-conditional image generation with clip latents. *arXiv preprint arXiv:2204.06125*, 2022.
- [34] R. Rombach, A. Blattmann, D. Lorenz, P. Esser, and B. Ommer. High-resolution image synthesis with latent diffusion models. In *Proceedings of the IEEE/CVF Conference on Computer Vision and Pattern Recognition*, pages 10684–10695, 2022.
- [35] N. Ruiz, Y. Li, V. Jampani, Y. Pritch, M. Rubinstein, and K. Aberman. Dreambooth: Fine tuning text-to-image diffusion models for subject-driven generation. arXiv preprint arXiv:2208.12242, 2022.
- [36] R. San-Roman, E. Nachmani, and L. Wolf. Noise estimation for generative diffusion models. *CoRR*, 2104, 2021.
- [37] C. Schuhmann and P. Bevan. Laion pop: 600,000 high-resolution images with detailed descriptions. https://huggingface.co/datasets/laion/laion-pop, 2023.
- [38] C. Schuhmann, R. Beaumont, R. Vencu, C. W. Gordon, R. Wightman, M. Cherti, T. Coombes, A. Katta, C. Mullis, M. Wortsman, P. Schramowski, S. R. Kundurthy, K. Crowson, L. Schmidt, R. Kaczmarczyk, and J. Jitsev. LAION-5b: An open large-scale dataset for training next generation image-text models. In *Thirty-sixth Conference on Neural Information Processing Systems Datasets and Benchmarks Track*, 2022.
- [39] N. Shazeer, A. Mirhoseini, K. Maziarz, A. Davis, Q. Le, G. Hinton, and J. Dean. Outrageously large neural networks: The sparsely-gated mixture-of-experts layer. arXiv preprint arXiv:1701.06538, 2017.

- [40] J. Sohl-Dickstein, E. A. Weiss, N. Maheswaranathan, and S. Ganguli. Deep unsupervised learning using nonequilibrium thermodynamics. *CoRR*, 1503, 2015.
- [41] J. Song, C. Meng, and S. Ermon. Denoising diffusion implicit models. In ICLR. OpenReview.net, 2021.
- [42] Y. Song, J. Sohl-Dickstein, D. P. Kingma, A. Kumar, S. Ermon, and B. Poole. Score-based generative modeling through stochastic differential equations. *CoRR*, 2011:13456, 2020.
- [43] Stability. Stable diffusion v1.5 model card, https://huggingface.co/runwayml/stable-diffusion-v1-5, 2022.
- [44] Stability. Stable diffusion v2 model card, stable-diffusion-2-depth, https://huggingface.co/stabilityai/stable-diffusion-2-depth, 2022.
- [45] J. Tan, M. Dvorožňák, D. Sýkora, and Y. Gingold. Decomposing time-lapse paintings into layers. *ACM Transactions on Graphics (TOG)*, 34(4):61:1–61:10, July 2015. doi: 10.1145/2766960. URL http://doi.acm.org/10.1145/2766960.
- [46] J. Tan, J.-M. Lien, and Y. Gingold. Decomposing images into layers via RGB-space geometry. *ACM Transactions on Graphics (TOG)*, 36(1):7:1–7:14, Nov. 2016. ISSN 0730-0301. doi: 10.1145/2988229. URL http://doi.acm.org/10.1145/2988229.
- [47] J. Tan, J. Echevarria, and Y. Gingold. Efficient palette-based decomposition and recoloring of images via rgbxy-space geometry. ACM Transactions on Graphics (TOG), 37(6):262:1–262:10, Dec. 2018. ISSN 0730-0301. doi: 10.1145/3272127.3275054.
- [48] J. Tan, S. DiVerdi, J. Lu, and Y. Gingold. Pigmento: Pigment-based image analysis and editing. *Transactions on Visualization and Computer Graphics (TVCG)*, 25(9), 2019. doi: 10.1109/TVCG.2018.2858238.
- [49] J. Tang, Y. Aksoy, C. Öztireli, M. Gross, and T. O. Aydın. Learning-based sampling for natural image matting. In *Proc. CVPR*, 2019.
- [50] Q. Wang, X. Bai, H. Wang, Z. Qin, and A. Chen. Instantid: Zero-shot identity-preserving generation in seconds. *arXiv preprint arXiv:2401.07519*, 2024.
- [51] M. Xia, X. Liu, and T.-T. Wong. Invertible grayscale. *ACM Transactions on Graphics* (SIGGRAPH Asia 2018 issue), 37(6):246:1–246:10, Nov. 2018.
- [52] M. Xiao, S. Zheng, C. Liu, Y. Wang, D. He, G. Ke, J. Bian, Z. Lin, and T.-Y. Liu. *Invertible Image Rescaling*, pages 126–144. Springer International Publishing, 2020. ISBN 9783030584528.
- [53] N. Xu, B. Price, S. Cohen, and T. Huang. Deep image matting. Mar. 2017. doi: 10.48550/ ARXIV.1703.03872.
- [54] X. Xu, Z. Wang, E. Zhang, K. Wang, and H. Shi. Versatile diffusion: Text, images and variations all in one diffusion model. *arXiv* preprint arXiv:2211.08332, 2022.
- [55] X. Xu, J. Guo, Z. Wang, G. Huang, I. Essa, and H. Shi. Prompt-free diffusion: Taking" text" out of text-to-image diffusion models. *arXiv preprint arXiv:2305.16223*, 2023.
- [56] J. Yao, X. Wang, S. Yang, and B. Wang. Vitmatte: Boosting image matting with pre-trained plain vision transformers. *Information Fusion*, 103:102091, 2024.
- [57] H. Ye, J. Zhang, S. Liu, X. Han, and W. Yang. Ip-adapter: Text compatible image prompt adapter for text-to-image diffusion models. 2023.
- [58] L. Zhang and M. Agrawala. Adding conditional control to text-to-image diffusion models. *arXiv preprint arXiv:2302.05543*, 2023.
- [59] S. Zhao, D. Chen, Y.-C. Chen, J. Bao, S. Hao, L. Yuan, and K.-Y. K. Wong. Uni-controlnet: All-in-one control to text-to-image diffusion models. *arXiv preprint arXiv:2305.16322*, 2023.
- [60] J.-Y. Zhu, T. Park, P. Isola, and A. A. Efros. Unpaired image-to-image translation using cycle-consistent adversarial networks. In *Computer Vision (ICCV)*, 2017 IEEE International Conference on, 2017.

A Padded RGB Channels

In the RGB channel of a transparent RGBA image, we refer to pixels that are completely invisible as "undefined" pixels, *i.e.*, pixels with alpha value strictly equal to zero. Since these pixels are strictly invisible, processing them with arbitrary color does not influence the appearance of images after alpha blending. Nevertheless, since neural networks tends to produce high-frequency patterns surrounding image edges, we avoid unnecessary edges in the RGB channels to avoid potential artifacts. We define a local Gaussion filter

$$G(\mathbf{I}_c)_p = \begin{cases} \phi(\mathbf{I}_c)_p & , \text{ if } (\mathbf{I}_a)_p > 0\\ (\mathbf{I}_c)_p & , \text{ otherwise} \end{cases}$$
 (10)

where $\phi(\cdot)$ is a standard Gaussian filter with 13 * 13 kernel, and p is pixel position. We perform this filter 64 times to completely propagate colors to all "undefined" pixels.

B Neural Network Architecture

The latent transparency encoder has exactly same neural network architecture with Stable Diffusion latent VAE encoder [31] (but the input contains 4 channels for RGBA). This model is trained from scratch. The output convolution layer is zero-initialized to avoid initial harmful noise.

The latent transparency decoder is a UNet. The encoding part of this UNet has same architecture as Stable Diffusion's latent VAE encoder, while the decoding part has same architecture as Stable Diffusion's VAE decoder. The input latent is added to the middle block, and all the encoder's feature maps are added to the input of each decoder block with skip connection. To be specific, assuming the input image is $512 \times 512 \times 3$ and the input latent is $64 \times 64 \times 4$, the feature map goes through $512 \times 512 \times 3 \rightarrow 512 \times 512 \times 128 \rightarrow 256 \times 256 \times 256 \rightarrow 128 \times 128 \times 512 \rightarrow 64 \times 64 \times 512$ where each \rightarrow is two resnet blocks. Then input latent is projected by a convolution layer to match channel and then added to the middle feature. Then the decoder goes through $64 \times 64 \times 512 \rightarrow 128 \times 128 \times 512 \rightarrow 256 \times 256 \times 256 \rightarrow 512 \times 512 \times 128 \rightarrow 512 \times 3$ and here each \rightarrow also adds the skip features from the encoder's corresponding layers.

C PatchGAN Discriminator

We use exactly same PatchGAN Discriminator architecture, learning objective, and training scheduling with Latent Diffusion VAE [34]. We directly use the python class *LPIPSWithDiscriminator* from their official code base (the input channel is set to 4). The generator side objective (from [34]) can be written as

$$\mathbb{L}_{\text{disc}}(\boldsymbol{z}) = \text{relu}(1 - D_{\text{disc}}(\boldsymbol{z})), \tag{11}$$

where z is a matrx with shape $h \times w \times 4$ and $\text{relu}(\cdot)$ is rectified linear unit. The $D_{\text{disc}}(\cdot)$ is a neural network with 5 convolution-normalization-silu layers $512 \times 512 \times 3 \rightarrow 512 \times 512 \times 64 \rightarrow 256 \times 256 \times 128 \rightarrow 128 \times 128 \times 256 \rightarrow 64 \times 64 \times 512 \rightarrow 64 \times 64 \times 1$ and the last layer is a patch-wise real/fake classification layer. The last layer does not use normalization and activation.

D Single Transparent Images

We present additional results for single transparent images, from Figure 16 to Figure 31.

E Multiple Transparent Layers

We present additional results for multiple transparent layers, from Figure 32 to Figure 34.

F Foreground-Conditioned Backgrounds

We present additional results for foreground-conditioned backgrounds, from Figure 35 to Figure 36.

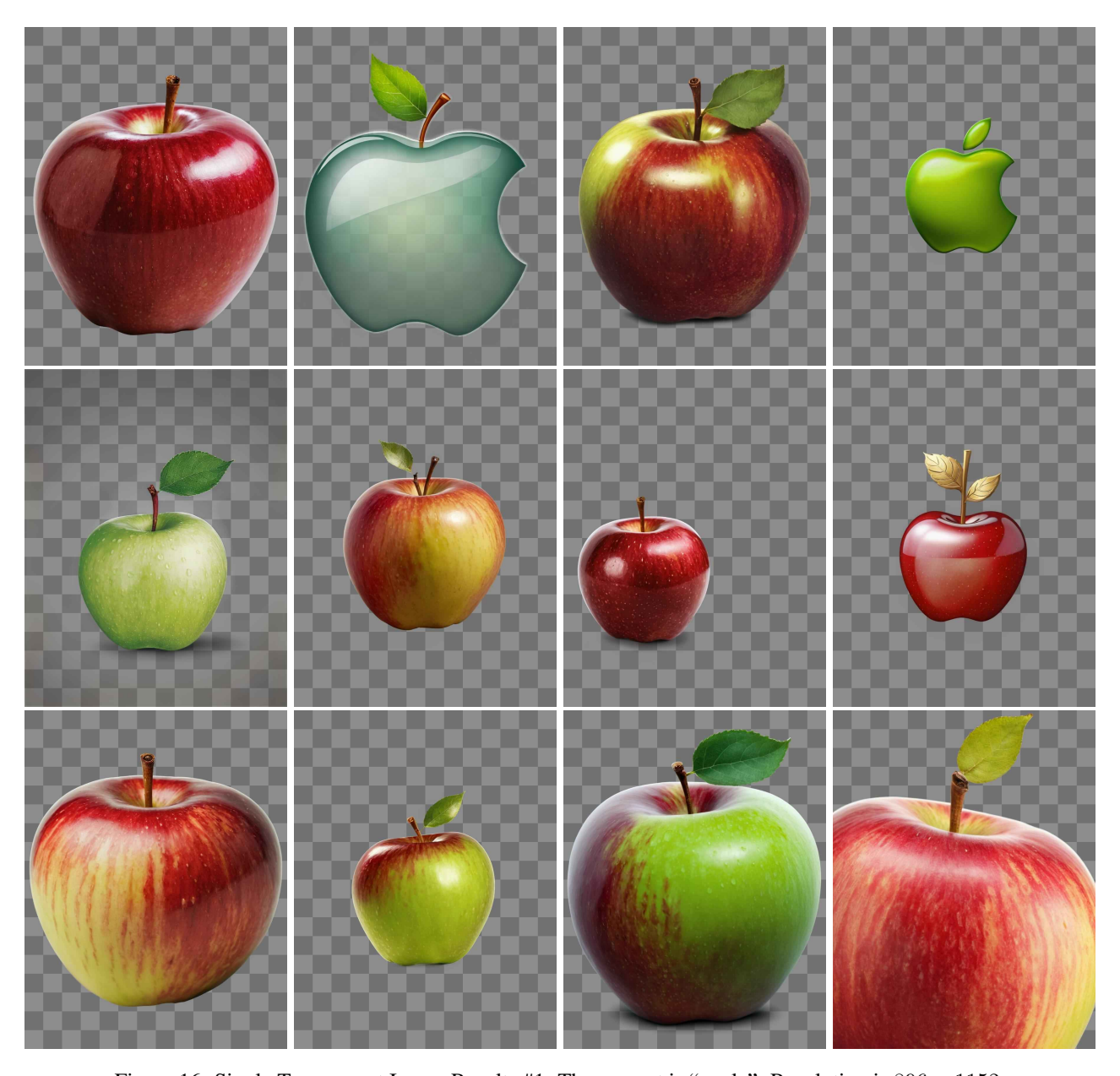


Figure 16: Single Transparent Image Results #1. The prompt is "apple". Resolution is 896×1152 .

G Background-Conditioned Foregrounds

We present additional results for background-conditioned foregrounds in Figure 37.

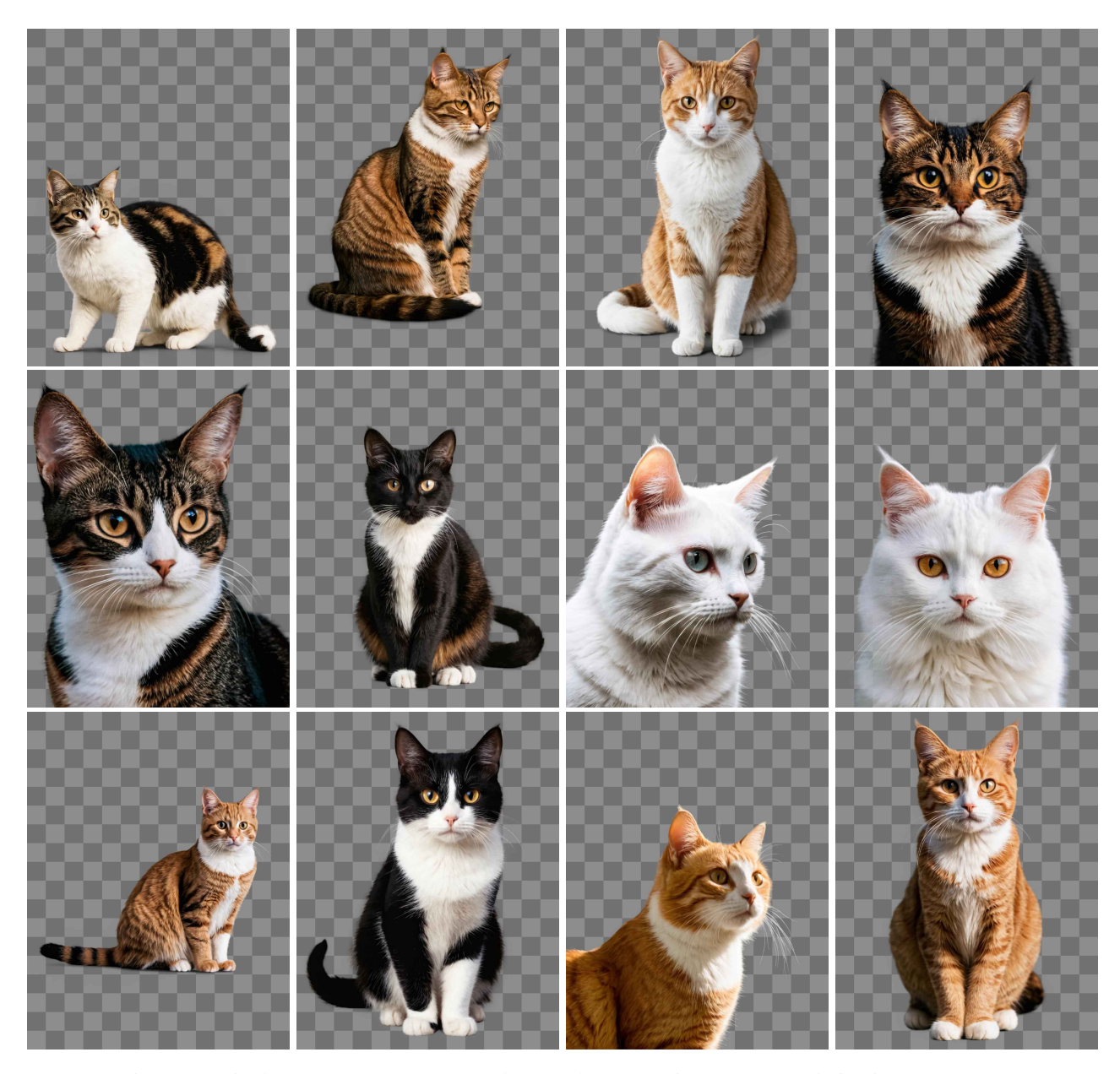


Figure 17: Single Transparent Image Results #2. The prompt is "a cat". Resolution is 896×1152 .



Figure 18: Single Transparent Image Results #3. The prompt is "a man". Resolution is 896×1152 .



Figure 19: Single Transparent Image Results #4. The prompt is "a man with messy hair". Resolution is 896×1152 .



Figure 20: Single Transparent Image Results #5. The prompt is "woman". Resolution is 896×1152 .



Figure 21: Single Transparent Image Results #6. The prompt is "woman with messy hair". Resolution is 896×1152 .

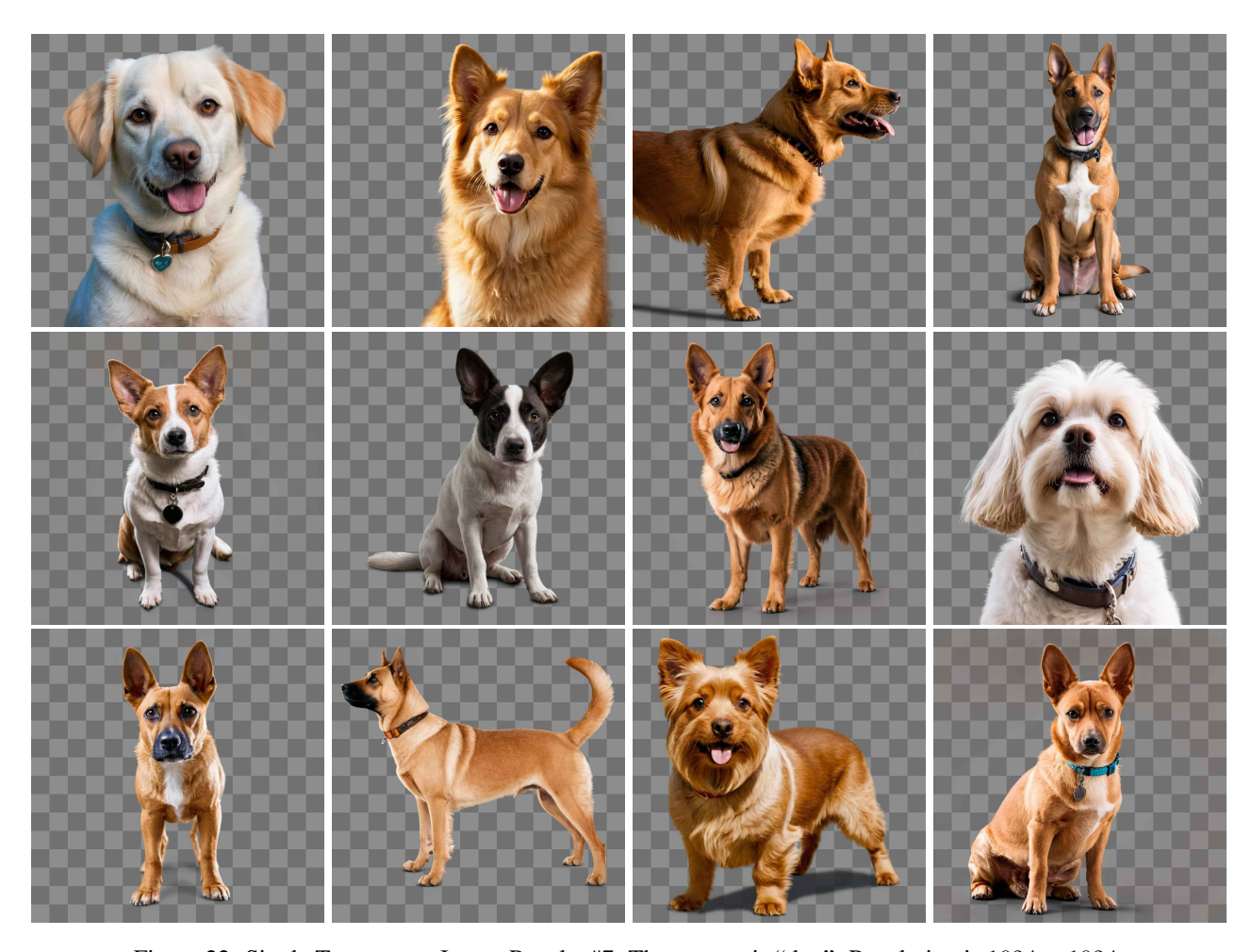


Figure 22: Single Transparent Image Results #7. The prompt is "dog". Resolution is 1024×1024 .



Figure 23: Single Transparent Image Results #8. The prompt is "glass cup". Resolution is 1024×1024 .



Figure 24: Single Transparent Image Results #9. The prompt is "dragon". Resolution is 1152×896 .



Figure 25: Single Transparent Image Results #10. The prompt is "car". Resolution is 1152×896 .



Figure 26: Single Transparent Image Results #11. The prompt is "magic book". Resolution is 1152×896 .

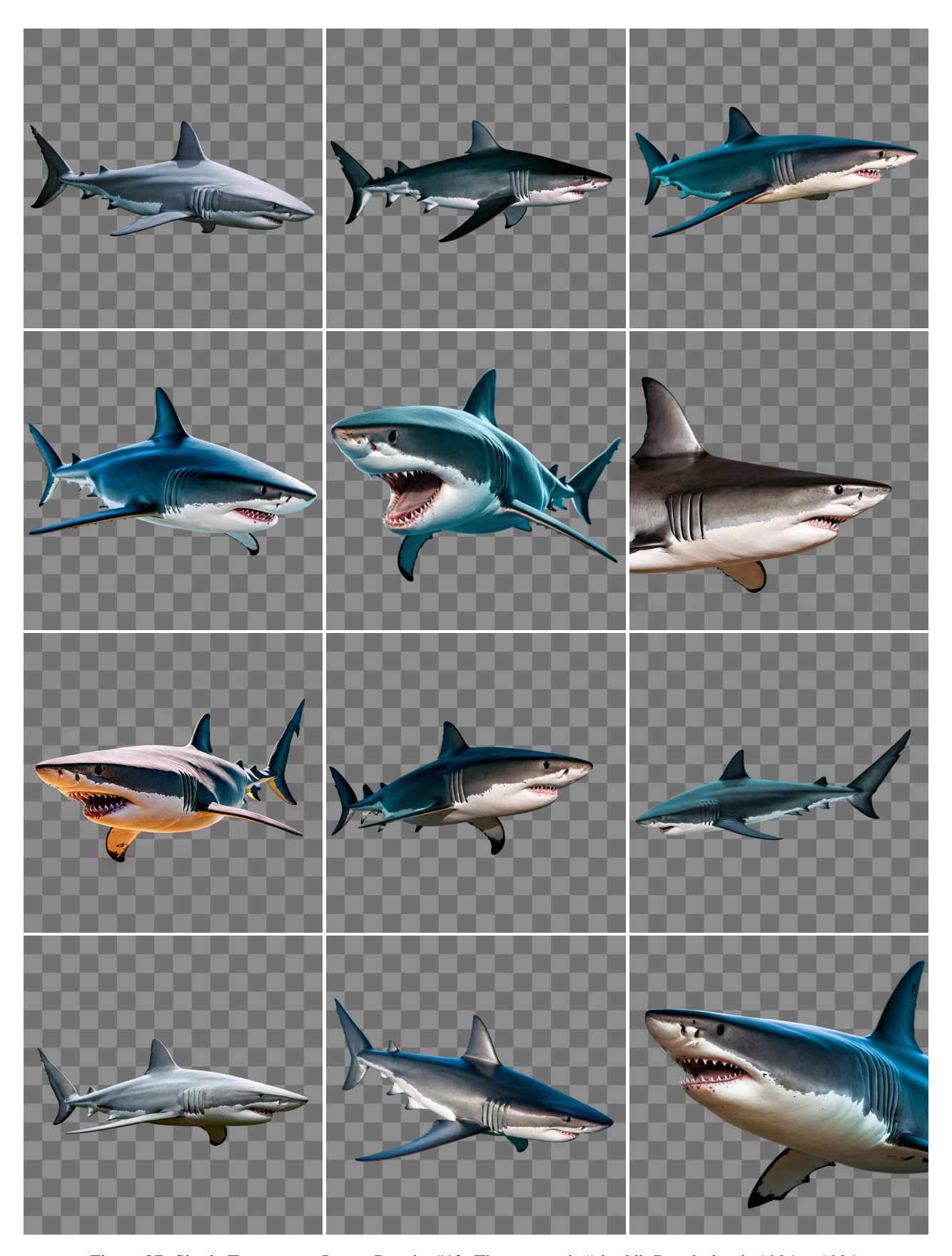


Figure 27: Single Transparent Image Results #12. The prompt is "shark". Resolution is 1024×1024 .



Figure 28: Single Transparent Image Results #13. The prompt is "magic stone". Resolution is 896×1152 .



Figure 29: Single Transparent Image Results #14. The prompt is "parrot, green fur". Resolution is 896×1152 .

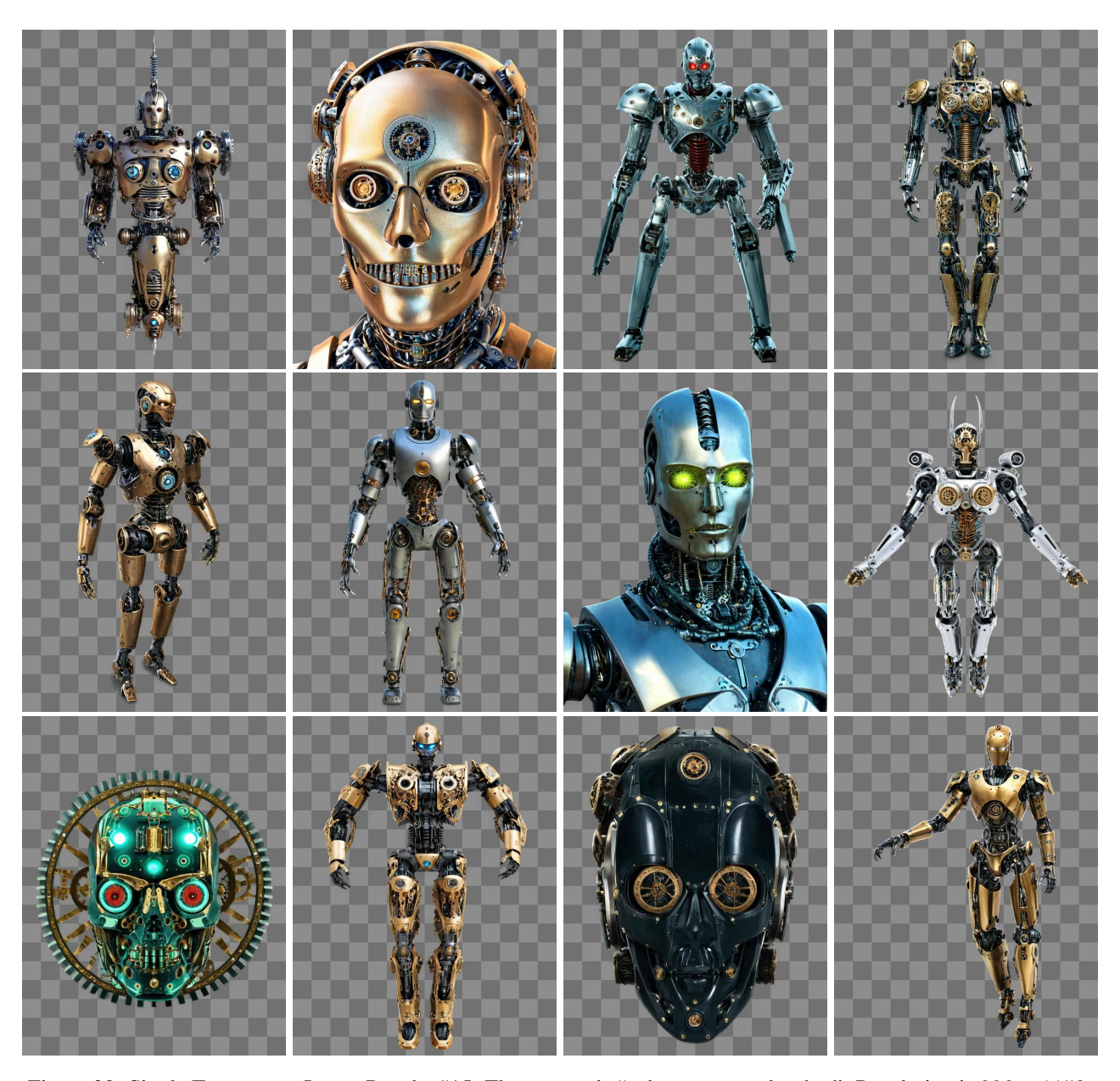


Figure 30: Single Transparent Image Results #15. The prompt is "cyber steampunk robot". Resolution is 896×1152 .



Figure 31: Single Transparent Image Results #16. The prompt is "necromancer". Resolution is 896×1152 .



Figure 32: Multi-layer Results #1. The prompts are "plant on table", "woman in room", "dog on floor", "man walking on street". Resolution is 896×1152 .

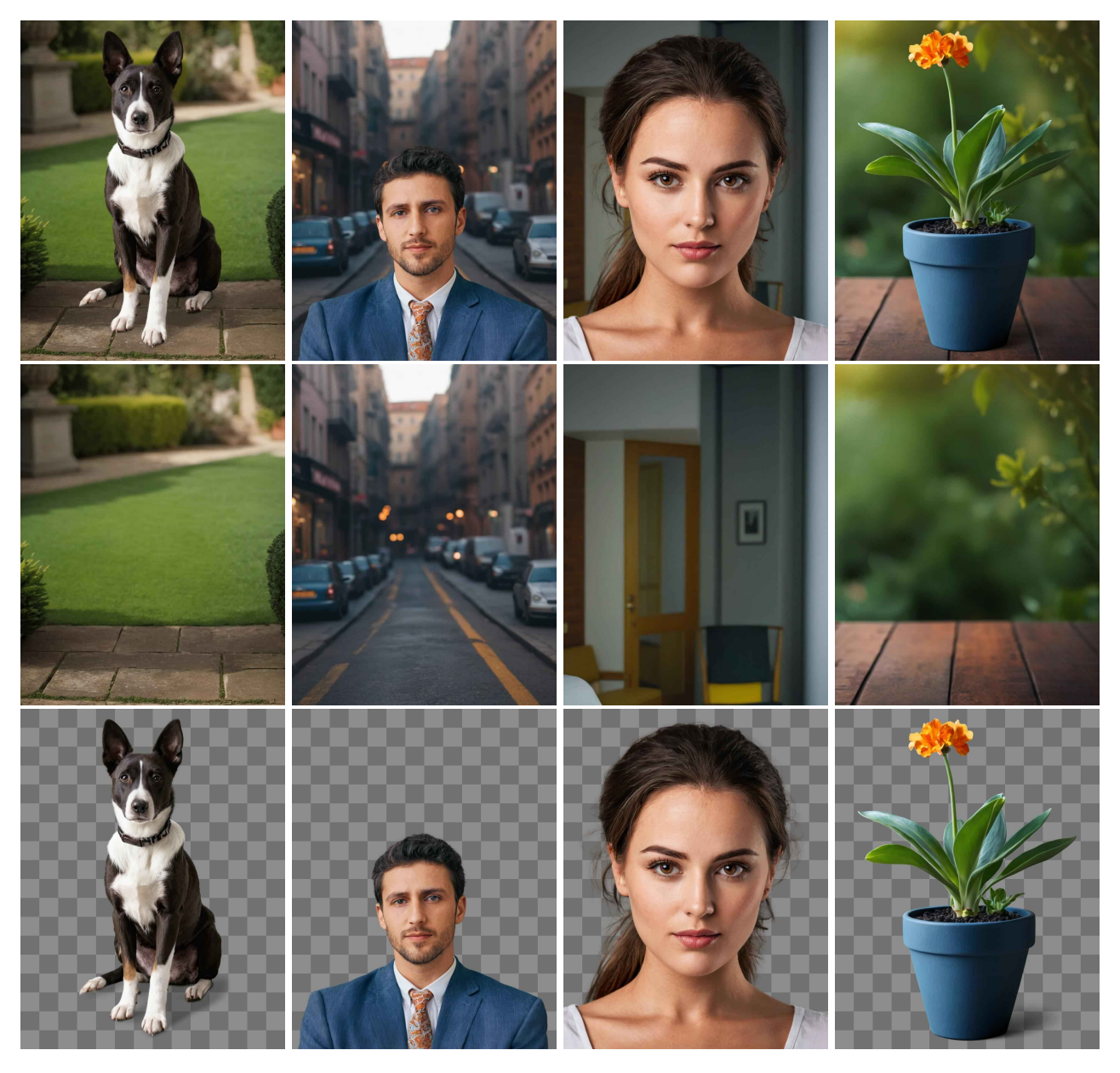


Figure 33: Multi-layer Results #2. The prompts are "dog in garden", "man in street", "woman, closeup", "plants on table". Resolution is 896×1152 .

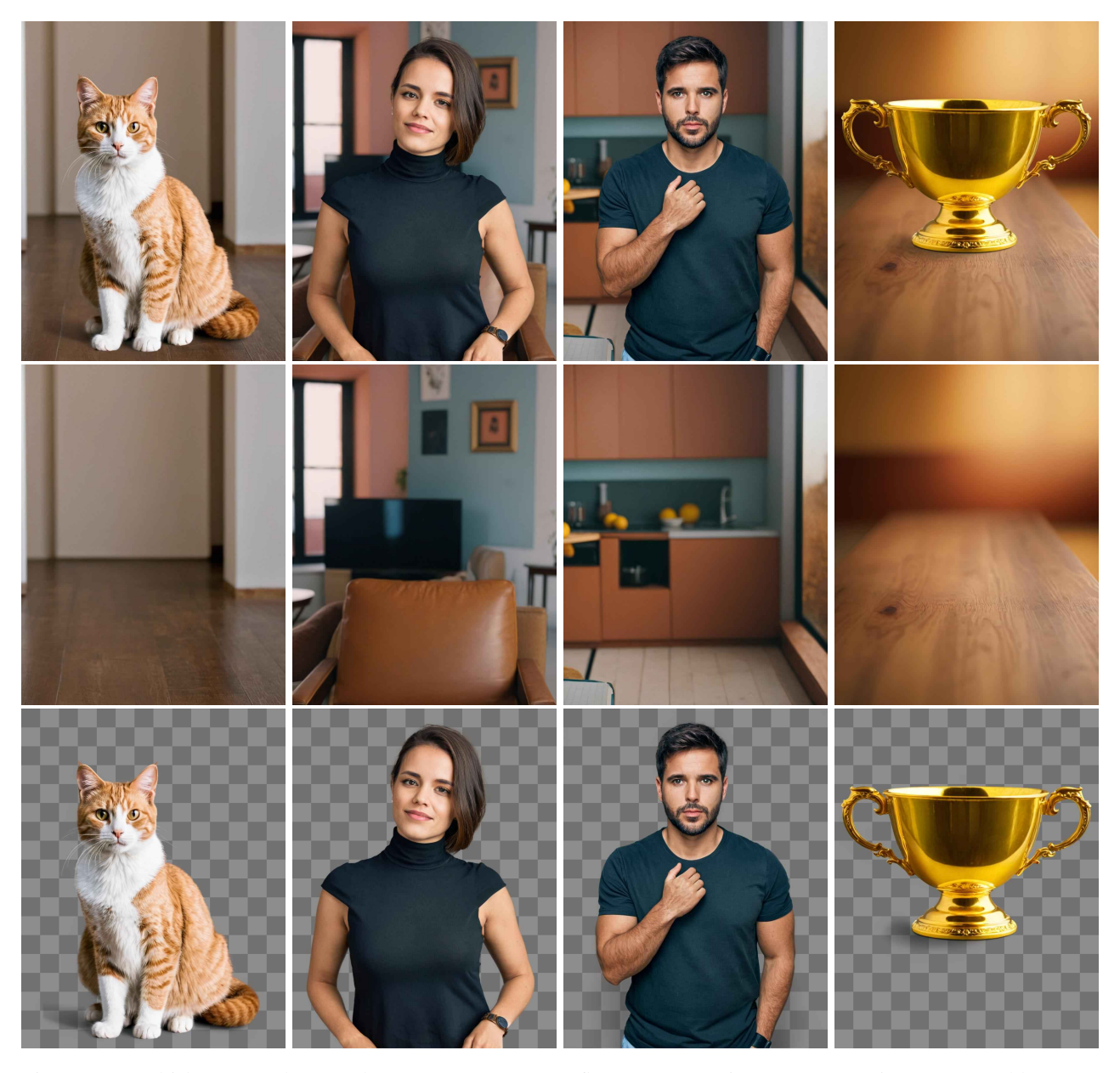


Figure 34: Multi-layer Results #3. The prompts are "cat on floor", "woman in room", "man in room", "golden cup". Resolution is 896×1152 .



Figure 35: Foreground-conditioned Background Results #1. The left-most images are inputs. The prompts are "man sitting on chair", "man sitting in forest", "pots on wood table", "parrot in room", "parrot in forest". Resolution is 896×1152 .



Figure 36: Foreground-conditioned Background Results #2. The left-most images are inputs. The prompts are "magic book of death", "magic book of life", "blue and white porcelain vase in my home", "blue and white porcelain vase in the museum", "the man in the snow", "god of infinity". Resolution is 896×1152 .



Figure 37: Background-conditioned Foreground Results #1. The left-most images are inputs. The prompts are "woman climbing mountain", "man climbing mountain", "robot in sofa waving hand", "man in sofa", "bird on hand", "apple on hand". Resolution is 896×1152 .